ÉCOLE POLYTECHNIQUE FÉDÉRALE DE LAUSANNE

MATHICSE

Mathematics Institute of Computational Science and Engineering

School of Basic Sciences - Section of Mathematics

MATHICSE Technical Report

Nr. 13.2015

Mai 2015 (NEW February 2016)

FaCSI: A block parallel preconditioner for fluid-structure interaction in hemodynamics

Simone Deparis, Davide Forti, Gwenol Grandperrin, Alfio Quarteroni

http://mathicse.epfl.ch

Phone: +41 21 69 37648

Address:
EPFL - SB - MATHICSE (Bâtiment MA)
Station 8 - CH-1015 - Lausanne - Switzerland

Fax: +41 21 69 32545

FaCSI: A Block Parallel Preconditioner for Fluid-Structure Interaction in Hemodynamics

Simone Deparis[a], Davide Forti[a,*], Gwenol Grandperrin[a], Alfio Quarteroni[a,b]

[a]*CMCS – Chair of Modeling and Scientific Computing*
MATHICSE – Mathematics Institute of Computational Science and Engineering
EPFL – École Polytechnique Fédérale de Lausanne
Station 8, Lausanne, CH–1015, Switzerland

[b]*MOX – Modeling and Scientific Computing*
Mathematics Department
Politecnico di Milano
via Bonardi 9, Milano, 20133, Italy (on leave)

Abstract

Modeling Fluid-Structure Interaction (FSI) in the vascular system is mandatory to reliably compute mechanical indicators in vessels undergoing large deformations. In order to cope with the computational complexity of the coupled 3D FSI problem after discretizations in space and time, a parallel solution is often mandatory. In this paper we propose a new block parallel preconditioner for the coupled linearized FSI system obtained after space and time discretization. We name it FaCSI to indicate that it exploits the factorized form of the linearized FSI matrix, the use of static condensation to formally eliminate the interface degrees of freedom of the fluid equations, and the use of a SIMPLE preconditioner for saddle-point problems. FaCSI is built upon a block Gauss-Seidel factorization of the FSI Jacobian matrix and it uses ad-hoc preconditioners for each physical component of the coupled problem, namely the fluid, the structure and the geometry. In the fluid subproblem, after operating static condensation of the interface fluid variables, we use a SIMPLE preconditioner on the reduced fluid matrix. Moreover, to efficiently deal with a large number of processes, FaCSI exploits efficient single field preconditioners, e.g., based on domain decomposition or the multigrid method. We measure the parallel performances of FaCSI on a benchmark cylindrical geometry and on a problem of physiological interest, namely the blood flow through a patient-specific femoropopliteal bypass. We analyse the dependence of the number of linear solver iterations on the cores count (scalability of the preconditioner) and on the mesh size (optimality).

Keywords: Fluid-structure interaction, scalable parallel preconditioners, finite element method, unstructured tetrahedral meshes, high performance computing, Navier-Stokes equations, hemodynamics

1. Introduction

In this paper we consider Fluid-Structure Interaction (FSI) problems for modeling blood flow in vessels undergoing relatively large deformations. In these cases, models based on rigid walls can not accurately predict key features of blood flow such as pressure wave propagation and arterial stresses. We are interested

*Corresponding author. E-mail: davide.forti@epfl.ch, Phone:+41 21 6930352, Fax:+41 21 6935510.

in the specific situation where the fluid is formulated in an Arbitrary Lagrangian Eulerian (ALE) frame of reference as in, e.g., [11, 14, 46, 24]. The ALE formulation satisfies exactly the coupling conditions on the fluid-structure interface at the expense of introducing a new equation for the fluid domain motion. An alternative approach to the ALE would be to formulate the FSI problem in a fully Eulerian frame of reference [13, 58], i.e. on a fixed fluid domain, but this additionally requires one to keep track of the position of the fluid-structure interface. Another approach is that of the immersed boundary method, where the fluid is written in Eulerian coordinates, while the structure is still in a Lagrangian frame of reference [50, 45]. See, e.g., [24, 11] and references therein for an overview of the subject.

The use of an ALE formulation for the fluid, together with a Lagrangian frame for the structure, yields an FSI problem that is composed by three subproblems, namely the *fluid problem*, which allows for the computation of the velocity and pressure inside the fluid domain, the *solid problem*, which describes the deformation of the vessel wall, and the so-called *geometry problem*, which accounts for the change in time of the computational fluid domain. A modular approach to solve the FSI problem would consist in dealing with the three problems separately. For example, one can consider the fluid-structure coupled problem using different type of interface conditions (Dirichlet-Neumann [40, 43], Robin-Robin [6, 5, 47], Neumann-Neumann, FETI, etc. [57]) to ensure the coupling. A further approach makes use of a Steklov-Poincaré formulation [17, 18] to enforce the coupling on the fluid-structure interface. Furthermore, one can also solve the coupled fluid-structure problem and, separately, the geometry one, therefore in two separate steps, as in the case of the so-called Geometry Convective Explicit (GCE) scheme [4, 14].

We consider the coupled problem as a single system involving all the state variables, including the fluid domain displacement. This system is nonlinear because of the convective term in the Navier-Stokes equations, the possible nonlinearity of the constitutive law used to model the vessel wall, and the changing-in-time fluid computational domain. The time discretization of the fluid problem is carried out by second order backward differentiation formulas, while for the structure we use the Newmark method. The spatial discretization is based on finite elements: we use $\mathbb{P}_2$-$\mathbb{P}_1$ Lagrange polynomials for the approximation of the fluid velocity and pressure, respectively, $\mathbb{P}_2$ for the structure displacement and $\mathbb{P}_2$ for the ALE map, using conforming meshes at the fluid-structure interface.

After spatial and time discretization we solve the fully coupled nonlinear FSI system in its implicit form by using the exact Newton method [8, 10, 20, 23, 31, 32, 39, 56]. Our choice relies on the fact that, in general, iterative algorithms (with convenient preconditioners) applied to the fully coupled FSI problem feature better convergence and higher computational efficiency. Other strategies may be employed to linearize the nonlinear FSI system: for instance, one can use relaxed fixed point iterations using Aitken acceleration [12, 40, 41, 43] or inexact Newton methods [28, 16], which may not converge or converge only linearly.

The numerical solution of the fully coupled 3D FSI problem is computationally expensive; to lower the time to solution, the use of an efficient preconditioner is crucial. In this regard, several strategies have been proposed in, e.g., [6, 7, 14, 26, 31, 59]. For instance, in [26], two preconditioners that apply algebraic multigrid techniques to the monolithically coupled fluid-structure interaction system are proposed. In the recent work [59], the solution of the linearized FSI coupled system is carried out by the GMRES method using a one level overlapping additive Schwarz preconditioner for the whole FSI Jacobian matrix.

In this work, we focus on block preconditioners: the mixed nature of the equations involving fluid, structure, and geometry motivates the development of preconditioners that are built upon the specific features of each of these three subproblems. These preconditioners enjoy the same modularity property of fully segregated methods where each subproblem is solved separately. Our block preconditioner FaCSI is constructed through the following steps. First, we consider a block Gauss-Seidel approximation of the FSI Jacobian

matrix: this amounts to drop the block associated to the kinematic coupling condition. This simplification can be reinterpreted as imposing (one-sided) Dirichlet boundary conditions on the structure displacement at the fluid-structure interface. Then, by a proper matrix factorization we identify three block-triangular matrices: the first matrix refers solely to the structural problem, the second one solely to the geometry and the last solely to the fluid. Special attention is paid to the fluid matrix whose saddle-point structure features the additional presence of two coupling blocks: after carrying out static condensation of the interface fluid variables, we use a SIMPLE preconditioner [19, 48, 49, 21, 22, 51, 52] on the reduced fluid matrix. Finally, on the approximate factorization, FaCSI is obtained by replacing the diagonal blocks referring to each physical subproblem by suitable parallel preconditioners, e.g, those based on domain decomposition or multigrid strategies. In particular, we show that FaCSI differs from the block Gauss-Seidel preconditioner proposed in [26].

As a first numerical example we solve a FSI problem on a benchmark cylindrical geometry. A comparative analysis of both the strong and weak scalability properties of FaCSI is carried out by using different preconditioners (algebraic additive Schwarz and algebraic multigrid) for the structure, geometry and fluid problems. Furthermore, we compare the performance of FaCSI with state of the art preconditioners for FSI [26, 59]. As a second example, we address a large-scale simulation of blood flow in a patient-specific femoropopliteal bypass.

The remainder of the paper is organized as follows. In Section 2, we describe the FSI model, introduce the weak form of the equations, and discretize them in time and space. Then, in Section 3, we address the numerical solution of the resulting nonlinear FSI system by the Newton method. In Section 4, we focus on the preconditioning strategy: in particular, we address the description of FaCSI and how it compares with preconditioners devised from other condensed formulations (see Section 4.2). Finally, numerical experiments aimed at studying the weak and strong scalability properties of FaCSI, as well as its computational performance, are presented in Section 5. Conclusions are drawn in Section 6.

2. Model description

We adopt the FSI model described in, e.g., [14, 15], which consists of a fluid governed by the incompressible Navier-Stokes equations written in the Arbitrary Lagrangian Eulerian (ALE) frame of reference, coupled with a structure modeled by linear elasticity. It is convenient to separate the FSI problem into three coupled subproblems, namely the fluid problem, the structure problem, and the geometry problem. The latter determines the displacement of the fluid domain $\hat{\mathbf{d}}_f$ which defines in turn the ALE map. We consider

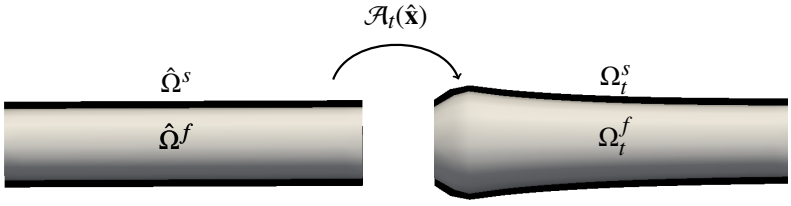

Figure 1: The ALE frame of reference.

$\hat{\mathbf{d}}_f$ as an harmonic extension to the fluid reference domain $\hat{\Omega}^f \subset \mathbb{R}^3$ of the trace of the solid displacement $\hat{\mathbf{d}}_s$ at the reference fluid-structure interface $\hat{\Gamma}$:

$$\begin{cases} -\Delta\hat{\mathbf{d}}_f = 0 & \text{in } \hat{\Omega}^f, \quad (1a) \\ \hat{\mathbf{d}}_f = \hat{\mathbf{d}}_s & \text{on } \hat{\Gamma}. \quad (1b) \end{cases}$$

The solution of the geometry problem defines the ALE map $\mathcal{A}_t(\hat{\mathbf{x}}) = \hat{\mathbf{x}} + \hat{\mathbf{d}}_f(\hat{\mathbf{x}}, t)\ \forall \hat{\mathbf{x}} \in \hat{\Omega}^f$, and the current fluid domain configuration. The Navier-Stokes equations for an incompressible fluid written in ALE coordinates read:

$$\begin{cases} \rho_f \left.\dfrac{\partial \mathbf{u}_f}{\partial t}\right|_{\hat{\mathbf{x}}} + \rho_f((\mathbf{u}_f - \mathbf{w}) \cdot \nabla)\mathbf{u}_f - \nabla \cdot \boldsymbol{\sigma}_f = 0 & \text{in } \Omega_t^f, \quad (2a) \\ \nabla \cdot \mathbf{u}_f = 0 & \text{in } \Omega_t^f, \quad (2b) \\ \mathbf{u}_f = \mathbf{h}_f & \text{on } \Gamma_D^f, \\ \boldsymbol{\sigma}_f \mathbf{n}_f = \mathbf{g}_f & \text{on } \Gamma_N^f, \\ \mathbf{u}_f \circ \mathcal{A}_t = \dfrac{\partial \hat{\mathbf{d}}_s}{\partial t} & \text{on } \hat{\Gamma}, \quad (2c) \end{cases}$$

where $\left.\dfrac{\partial}{\partial t}\right|_{\hat{\mathbf{x}}} = \dfrac{\partial}{\partial t} + \mathbf{w} \cdot \nabla$ is the ALE derivative, $\mathbf{w}(\mathbf{x}) = \dfrac{\partial \mathcal{A}_t(\mathbf{x})}{\partial t}$ is fluid domain velocity, $\mathbf{u}_f$ and p_f are the velocity and pressure of the fluid, respectively. In (2a) we denoted by ρ_f the density of the fluid and by $\boldsymbol{\sigma}_f$ the Cauchy stress tensor

$$\boldsymbol{\sigma}_f = \mu_f(\nabla \mathbf{u}_f + (\nabla \mathbf{u}_f)^T) \ - \ p_f \mathbf{I},$$

with $\mathbf{I}$ being the identity tensor, μ_f the dynamic viscosity of the fluid, and $\mathbf{n}_f$ the outward unit normal vector to $\partial\Omega_t^f$. The functions $\mathbf{h}_f$ and $\mathbf{g}_f$ indicate the Dirichlet and Neumann data applied at the the Dirichlet and Neumann boundaries Γ_D^f and Γ_N^f, respectively, of Ω_t^f.

In this work we model the structure by linear elasticity in a Lagrangian frame of reference:

$$\begin{cases} \hat{\rho}_s \dfrac{\partial^2 \hat{\mathbf{d}}_s}{\partial t^2} - \nabla_{\hat{\mathbf{x}}} \cdot \boldsymbol{\Pi}(\hat{\mathbf{d}}_s) = 0 & \text{in } \hat{\Omega}^s, \quad (3a) \\ \hat{\mathbf{d}}_s = \mathbf{h}_s & \text{on } \hat{\Gamma}_D^s, \\ \boldsymbol{\Pi}(\hat{\mathbf{d}}_s)\hat{\mathbf{n}}_s = 0 & \text{on } \hat{\Gamma}_N^s, \\ \boldsymbol{\Pi}(\hat{\mathbf{d}}_s)\hat{\mathbf{n}}_s + \hat{\boldsymbol{\sigma}}_f \hat{\mathbf{n}}_f = 0 & \text{on } \hat{\Gamma}. \quad (3b) \end{cases}$$

Here $\hat{\mathbf{n}}_s$ and $\hat{\mathbf{n}}_f$ represent the outward unit normal vector to $\partial\hat{\Omega}_s$ and $\partial\hat{\Omega}_f$, respectively, $\hat{\boldsymbol{\sigma}}_f = (\det[\mathbf{F}])\, \mathbf{F}^{-T}\, \boldsymbol{\sigma}_f$ and $\mathbf{F} = \mathbf{I} + \nabla_{\hat{\mathbf{x}}} \hat{\mathbf{d}}_s$ is the deformation gradient tensor. The function $\mathbf{h}_s$ indicates the Dirichlet data applied at the Dirichlet boundary Γ_D^s of $\hat{\Omega}^s$. The material is characterized by the Young modulus E_s and the Poisson ratio ν_s, which define in turn the first Piola-Kirchhoff stress tensor

$$\boldsymbol{\Pi}(\hat{\mathbf{d}}_s) = \lambda_s \operatorname{Tr}\left(\frac{\nabla \hat{\mathbf{d}}_s + (\nabla \hat{\mathbf{d}}_s)^T}{2}\right)\mathbf{I} + \mu_s(\nabla \hat{\mathbf{d}}_s + (\nabla \hat{\mathbf{d}}_s)^T),$$

where

$$\lambda_s = \frac{E_s \nu_s}{(1 - 2\nu_s)(1 + \nu_s)}, \qquad \mu_s = \frac{E_s}{2(1 + \nu_s)}.$$

The coupling between these three subproblems is ensured by imposing the geometry adherence, the continuity of the velocity and the continuity of the normal stresses at the interface through Equations (1b), (2c), and (3b), respectively. The resulting system is nonlinear due to the convective term in the fluid momentum equation and to the moving fluid domain.

2.1. Weak formulation

We follow [46, 41] to derive the weak form of the FSI problem in the nonconservative form. The velocity coupling condition is imposed strongly, while the continuity of the normal stresses is imposed in weak form. Let us introduce the following functional spaces:

$$
\begin{aligned}
U^f &= \{\mathbf{v} = \hat{\mathbf{v}} \circ \mathcal{A}_t^{-1} \mid \hat{\mathbf{v}} \in [H^1(\hat{\Omega}^f)]^3\},\\
U_D^f &= \{\mathbf{v} = \hat{\mathbf{v}} \circ \mathcal{A}_t^{-1} \mid \hat{\mathbf{v}} \in [H^1(\hat{\Omega}^f)]^3, \hat{\mathbf{v}} = 0 \text{ on } \Gamma_D^f\},\\
Q^f &= \{q = \hat{q} \circ \mathcal{A}_t^{-1} \mid \hat{q} \in L^2(\hat{\Omega}^f)\},\\
U^s &= [H^1(\hat{\Omega}^s)]^3,\ U_D^s = \{\mathbf{v} \in [H^1(\hat{\Omega}^s)]^3 \mid \mathbf{v} = 0 \text{ on } \Gamma_D^s\},\\
U^g &= [H^1(\hat{\Omega}^f)]^3,\ U_D^g = \{\mathbf{v} \in [H^1(\hat{\Omega}^f)]^3 \mid \mathbf{v} = 0 \text{ on } \Gamma_{fixed}^f\},\\
U^\lambda &= [H^{-1/2}(\hat{\Gamma})]^3.
\end{aligned}
$$

The weak form of the fluid and structure equations is standard [14]. We introduce an auxiliary variable $\boldsymbol{\lambda} \in U^\lambda$

$$
\boldsymbol{\lambda} := \hat{\sigma}_f \hat{\mathbf{n}}_f = -\Pi(\hat{\mathbf{d}}_s)\hat{\mathbf{n}}_s \qquad \text{in } U^\lambda, \tag{4}
$$

that can be regarded as a set of Lagrange multipliers used to enforce the continuity of the velocity at the interface.

We recall the notation for the Dirichlet boundary data for the fluid, structure and geometry subproblem: $\mathbf{h}_f : \Gamma_D^f \to \mathbb{R}^2$, $\mathbf{h}_s : \Gamma_D^s \to \mathbb{R}^2$, $\mathbf{h}_g : \Gamma_{fixed}^f \to \mathbb{R}^2$, respectively. The weak form of the FSI problem reads: for all $t \in (0, T]$, find $\mathbf{u}_f \in U^f$ such that $\mathbf{u}_f = \mathbf{h}_f$ on Γ_D^f, $p_f \in Q^f$, $\hat{\mathbf{d}}_s \in U^s$ such that $\hat{\mathbf{d}}_s = \mathbf{h}_s$ on Γ_D^s, $\hat{\mathbf{d}}_f \in U^g$ such that $\hat{\mathbf{d}}_f = \mathbf{h}_g$ on Γ_{fixed}^f, and $\boldsymbol{\lambda} \in U^\lambda$ satisfying

$$
\begin{aligned}
\int_{\Omega_t^f} \left(\rho_f \left.\frac{\partial \mathbf{u}_f}{\partial t}\right|_{\hat{\mathbf{x}}} \cdot \mathbf{v}_f + \rho_f((\mathbf{u}_f - \mathbf{w}) \cdot \nabla)\mathbf{u}_f \cdot \mathbf{v}_f + \boldsymbol{\sigma}_f : \nabla \mathbf{v}_f \right) d\Omega_t^f + \int_{\hat{\Gamma}} \boldsymbol{\lambda} \cdot (\mathbf{v}_f \circ \mathcal{A}_t)\, d\hat{\gamma} & \\
= \int_{\Gamma_N^f} \mathbf{g}_f \cdot \mathbf{v}_f \, d\gamma \qquad \forall \mathbf{v}_f \in U_D^f, & \\
\int_{\Omega_t^f} q\, \nabla \cdot \mathbf{u}_f \, d\Omega_t^f = 0 \qquad \forall q \in Q^f, & \\
\int_{\hat{\Omega}^s} \left(\hat{\rho}_s \frac{\partial^2 \hat{\mathbf{d}}_s}{\partial t^2} \cdot \mathbf{v}_s + \Pi(\hat{\mathbf{d}}_s) : \nabla_{\hat{\mathbf{x}}} \mathbf{v}_s \right) d\hat{\Omega}^s - \int_{\hat{\Gamma}} \boldsymbol{\lambda} \cdot \mathbf{v}_s \, d\hat{\gamma} = \int_{\Gamma_N^s} \mathbf{g}_s \cdot \mathbf{v}_s \, d\gamma \qquad \forall \mathbf{v}_s \in U_D^s, & \qquad (5)\\
\int_{\hat{\Gamma}} (\mathbf{u}_f \circ \mathcal{A}_t) \cdot \boldsymbol{\eta} \, d\gamma - \int_{\hat{\Gamma}} \frac{\partial \hat{\mathbf{d}}_s}{\partial t} \cdot \boldsymbol{\eta} \, d\gamma = 0 \qquad \forall \boldsymbol{\eta} \in [H^{-1/2}(\hat{\Gamma})]^3, & \\
\int_{\hat{\Gamma}} \nabla_{\hat{\mathbf{x}}} \hat{\mathbf{d}}_f : \nabla_{\hat{\mathbf{x}}} \mathbf{v}_g \, d\hat{\Omega}^f = 0 \qquad \forall \mathbf{v}_g \in U_D^g, & \\
\hat{\mathbf{d}}_f = \hat{\mathbf{d}}_s \qquad \text{on } \hat{\Gamma}, &
\end{aligned}
$$

where $\mathbf{w} = \dfrac{\partial \hat{\mathbf{d}}_f}{\partial t}$ represents the rate of deformation of the fluid domain.

Remark 1. In system (5) integrals on $\hat{\Gamma}$ should be intended in the sense of the duality.

2.2. Time and spatial discretization

We consider a Fully Implicit (FI) scheme for which all the nonlinearities are treated implicitly. We discretize the time derivative of the fluid problem by second order backward differentation formulas [25]

$$\left.\frac{\partial \mathbf{u}_f}{\partial t}(t^{n+1})\right|_{\hat{\mathbf{x}}} \approx \frac{3\mathbf{u}^{n+1} - 4\mathbf{u}^n + \mathbf{u}^{n-1}}{2\Delta t}. \tag{6}$$

The time discretization of the structural problem is carried out by the Newmark method [33]

$$\frac{\partial^2 \hat{\mathbf{d}}_s}{\partial t^2}(t^{n+1}) \approx \frac{1}{\beta \Delta t^2}\hat{\mathbf{d}}_s^{n+1} - \frac{1}{\beta \Delta t^2}(\hat{\mathbf{d}}_s^n + \Delta t\, \dot{\hat{\mathbf{d}}}_s^n) - \frac{1-2\beta}{2\beta}\, \ddot{\hat{\mathbf{d}}}_s^n, \tag{7}$$

where:

$$\ddot{\hat{\mathbf{d}}}_s^n = \frac{1}{\beta \Delta t^2}\hat{\mathbf{d}}_s^n - \frac{1}{\beta \Delta t^2}(\hat{\mathbf{d}}_s^{n-1} + \Delta t\, \dot{\hat{\mathbf{d}}}_s^{n-1}) - \frac{1-2\beta}{2\beta}\, \ddot{\hat{\mathbf{d}}}_s^{n-1}, \tag{8}$$

$$\dot{\hat{\mathbf{d}}}_s^n = \dot{\hat{\mathbf{d}}}_s^{n-1} + \Delta t\,(\gamma\, \ddot{\hat{\mathbf{d}}}_s^n + (1-\gamma)\, \ddot{\hat{\mathbf{d}}}_s^{n-1}). \tag{9}$$

We choose the coefficients $\gamma = 0.5$ and $\beta = 0.25$ such that the scheme is unconditionally stable and second order. In space, we consider a Galerkin finite elements approximation using $\mathbb{P}_2$-$\mathbb{P}_1$ Lagrange polynomials for the representation of the fluid variables $\mathbf{u}_f$ and p_f, respectively, $\mathbb{P}_2$ for the structure displacement $\hat{\mathbf{d}}_s$, and $\mathbb{P}_2$ for the harmonic extension $\hat{\mathbf{d}}_f$. At each time step, the resulting nonlinear system to be solved may be rewritten as

$$\begin{pmatrix} S(\hat{\mathbf{d}}_s^{n+1}) & + & 0 & + & 0 & - & I_{\Gamma^s}^T \boldsymbol{\lambda}^{n+1} \\ -I_{\Gamma^s}\hat{\mathbf{d}}_s^{n+1} & + & G(\hat{\mathbf{d}}_f^{n+1}) & + & 0 & + & 0 \\ 0 & + & 0 & + & F(\mathbf{u}_f^{n+1}, p_f^{n+1}, \hat{\mathbf{d}}_f^{n+1}) & + & I_{\Gamma^f}^T \boldsymbol{\lambda}^{n+1} \\ -\dfrac{\gamma}{\beta \Delta t}\, I_{\Gamma^s}\hat{\mathbf{d}}_s^{n+1} & + & 0 & + & I_{\Gamma^f}\mathbf{u}_f^{n+1} & + & 0 \end{pmatrix} = \begin{pmatrix} \mathbf{b}_s \\ 0 \\ \mathbf{b}_f \\ \mathbf{b}_c \end{pmatrix}. \tag{10}$$

We denoted by $\hat{\mathbf{d}}_s^{n+1}$, $\hat{\mathbf{d}}_f^{n+1}$, $\mathbf{u}_f^{n+1}$, p_f^{n+1}, and $\boldsymbol{\lambda}^{n+1}$, the unknown displacement of the structure, the displacement of the fluid domain, the velocity and pressure of the fluid, and the Lagrange multipliers, respectively. We make use of an augmented formulation wherein the vector of Lagrange multipliers $\boldsymbol{\lambda}^{n+1}$ is used to impose the continuity of the velocity at the fluid-structure interface. We notice that the Lagrange multipliers may formally be removed from the set of unknowns of the problem by static condensation, as in [26, 44]. However, we remark that we do not perform static condensation at this stage beacuse it would lead to additional implementation difficulties in our code library.

The diagonal blocks on the left hand side of (10) account for the discretized solid, geometry and fluid problems. We remark that F is nonlinear due to the convective term and the fact that fluid domain moves. The matrices I_{Γ^f} and I_{Γ^s} are the restriction of fluid and structure vectors to the interface and in (10) account for the continuity of velocities and the geometry adherence, which are imposed strongly. Their transposes account for the continuity of the normal stresses, which is imposed weakly. Last row of (10) represents the discretized kinematic coupling condition at the fluid-structure interface:

$$I_{\Gamma^f}\mathbf{u}_f - \frac{\gamma}{\beta \Delta t} I_{\Gamma^s}\hat{\mathbf{d}}_s^{n+1} = \mathbf{b}_c \quad \text{on } \hat{\Gamma}, \tag{11}$$

where

$$\mathbf{b}_c = I_{\Gamma^s}\dot{\hat{\mathbf{d}}}_s^n - \frac{\gamma}{\beta \Delta t}(I_{\Gamma^s}\hat{\mathbf{d}}_s^n + \Delta t\, I_{\Gamma^s}\dot{\hat{\mathbf{d}}}_s^n) - \Delta t\, \gamma \frac{1-2\beta}{2\beta}\, I_{\Gamma^s}\ddot{\hat{\mathbf{d}}}_s^n + \Delta t\,(1-\gamma)\, I_{\Gamma^s}\ddot{\hat{\mathbf{d}}}_s^n. \tag{12}$$

3. Numerical solution

We solve the nonlinear fully coupled FSI problem (10) using the Newton method as in, e.g., [23, 56, 31, 10, 8]. Let us denote the solution of (10) at time $t^n = n\,\Delta t$ by $\mathbf{X}^n = (\hat{\mathbf{d}}_s^n, \hat{\mathbf{d}}_f^n, \mathbf{u}_f^n, p_f^n, \boldsymbol{\lambda}^n)^T$. At each timestep, we compute a sequence of approximations $\mathbf{X}_1^{n+1}$, $\mathbf{X}_2^{n+1}$, etc. until the numerical solution converges up to a prescribed tolerance. The generic $k+1$ iteration of the Newton method applied to (10) is described as follows. Starting from an approximation of $\mathbf{X}_k^{n+1}$, we compute the residual $\mathbf{R}_k^{n+1} = (\mathbf{r}_{\mathbf{d}_s,k}^{n+1}, \mathbf{r}_{\mathbf{d}_f,k}^{n+1}, \mathbf{r}_{u_f,k}^{n+1}, r_{p_f,k}^{n+1}, \mathbf{r}_{\boldsymbol{\lambda},k}^{n+1})^T$:

$$\mathbf{R}_k^{n+1} = \begin{pmatrix} \mathbf{b}_s \\ 0 \\ \mathbf{b}_f \\ \mathbf{b}_c \end{pmatrix} - \begin{pmatrix} S(\hat{\mathbf{d}}_{s,k}^{n+1}) - I_{\Gamma^s}^T \boldsymbol{\lambda}_k^{n+1} \\ -I_{\Gamma^s}\hat{\mathbf{d}}_{s,k}^{n+1} + G(\hat{\mathbf{d}}_{f,k}^{n+1}) \\ F(\mathbf{u}_{f,k}^{n+1}, p_{f,k}^{n+1}, \hat{\mathbf{d}}_{f,k}^{n+1}) + I_{\Gamma^f}^T \boldsymbol{\lambda}_k^{n+1} \\ -\dfrac{\gamma}{\beta\Delta t} I_{\Gamma^s}\hat{\mathbf{d}}_{s,k}^{n+1} + I_{\Gamma^f}\mathbf{u}_{f,k}^{n+1} \end{pmatrix}. \tag{13}$$

Then, we compute the Newton correction vector $\delta\mathbf{X}_k^{n+1} = (\delta\hat{\mathbf{d}}_{s,k}^{n+1}, \delta\hat{\mathbf{d}}_{f,k}^{n+1}, \delta\mathbf{u}_{f,k}^{n+1}, \delta p_{f,k}^{n+1}, \delta\boldsymbol{\lambda}_k^{n+1})^T$ by solving the Jacobian linear system

$$J_{FSI}\,\delta\mathbf{X}_k^{n+1} = -\mathbf{R}_k^{n+1}, \tag{14}$$

being

$$J_{FSI} = \begin{pmatrix} \mathcal{S} & 0 & 0 & -I_{\Gamma^s}^T \\ -I_{\Gamma^s} & \mathcal{G} & 0 & 0 \\ 0 & \mathcal{D} & \mathcal{F} & I_{\Gamma^f}^T \\ -\dfrac{\gamma}{\beta\Delta t} I_{\Gamma^s} & 0 & I_{\Gamma^f} & 0 \end{pmatrix}, \tag{15}$$

where $\mathcal{S}$, $\mathcal{G}$ and $\mathcal{F}$ represents the linearized structure, geometry and fluid problems, respectively; $\mathcal{D}$ are the shape derivatives, i.e. the derivatives of $F(\mathbf{u}_f^{n+1}, p_f^{n+1}, \hat{\mathbf{d}}_f^{n+1})$ with respect to $\hat{\mathbf{d}}_f^{n+1}$ (for their exact computation see [23]).

Finally, we update the solution: $\mathbf{X}_{k+1}^{n+1} = \mathbf{X}_k^{n+1} + \delta\mathbf{X}_k^{n+1}$. We stop the Newton iterations when

$$\frac{\|\mathbf{R}_k^{n+1}\|_\infty}{\|\mathbf{R}_0^{n+1}\|_\infty} \leq \epsilon, \tag{16}$$

where $\mathbf{R}_0^{n+1}$ is the residual at the first Newton iteration and ϵ is a given tolerance.

4. Preconditioning strategy

In analogy with what is proposed in [14], we exploit the block structure of the Jacobian matrix associated to the fully coupled FSI problem (10) to build our preconditioner:

$$J_{FSI} = \begin{pmatrix} \boxed{\mathcal{S}} & 0 & 0 & -I_{\Gamma^s}^T \\ -I_{\Gamma^s} & \boxed{\mathcal{G}} & 0 & 0 \\ 0 & \mathcal{D} & \boxed{\begin{matrix} \mathcal{F} & I_{\Gamma^f}^T \\ I_{\Gamma^f} & 0 \end{matrix}} \\ -\dfrac{\gamma}{\beta\Delta t} I_{\Gamma^s} & 0 & \end{pmatrix},$$

which is lower block triangular up to the $-I_{\Gamma^s}^T$ block. By neglecting this block, we obtain the following Gauss-Seidel preconditioner for the matrix J_{FSI}:

$$P_{FSI} = \begin{pmatrix} \mathcal{S} & 0 & 0 & \boxed{0} \\ -I_{\Gamma^s} & \mathcal{G} & 0 & 0 \\ 0 & \mathcal{D} & \mathcal{F} & I_{\Gamma^f}^T \\ -\dfrac{\gamma}{\beta\Delta t} I_{\Gamma^s} & 0 & I_{\Gamma^f} & 0 \end{pmatrix}. \tag{17}$$

Having dropped $-I_{\Gamma^s}^T$ in J_{FSI} amounts to neglect the kinematic coupling condition: more precisely this can be reinterpreted as imposing (one-sided) Dirichlet boundary conditions on $\hat{\mathbf{d}}_s$ at the fluid-structure interface. A similar strategy was used for a Geometry Convective Explicit (GCE) scheme in [14]. If we assume that Dirichlet boundary conditions are imposed on at least a subset of the boundary of the structure domain, both $\mathcal{S}$ and P_{FSI} are nonsingular. In that case P_{FSI} can be factorized into three physics-specific nonsingular matrices, namely $P_{\mathcal{S}}$, $P_{\mathcal{G}}$, and $P_{\mathcal{F}}$ corresponding to the structure, the geometry, and the fluid problem, respectively:

$$P_{FSI} = \underbrace{\begin{pmatrix} \boxed{\mathcal{S}} & 0 & 0 & 0 \\ 0 & I & 0 & 0 \\ 0 & 0 & I & 0 \\ 0 & 0 & 0 & I \end{pmatrix}}_{P_{\mathcal{S}}} \underbrace{\begin{pmatrix} I & 0 & 0 & 0 \\ -I_{\Gamma^s} & \boxed{\mathcal{G}} & 0 & 0 \\ 0 & 0 & I & 0 \\ 0 & 0 & 0 & I \end{pmatrix}}_{P_{\mathcal{G}}} \underbrace{\begin{pmatrix} I & 0 & 0 & 0 \\ 0 & I & 0 & 0 \\ 0 & \mathcal{D} & \boxed{\mathcal{F}} & \boxed{I_{\Gamma^f}^T} \\ -\dfrac{\gamma}{\beta\Delta t} I_{\Gamma^s} & 0 & \boxed{I_{\Gamma^f}} & \boxed{0} \end{pmatrix}}_{P_{\mathcal{F}}}. \tag{18}$$

$P_{\mathcal{S}}$ is block diagonal while both $P_{\mathcal{G}}$ and $P_{\mathcal{F}}$ can be furtherly factorized into matrices featuring simpler block structures:

$$P_{\mathcal{G}} = \begin{pmatrix} I & 0 & 0 & 0 \\ -I_{\Gamma^s} & I & 0 & 0 \\ 0 & 0 & I & 0 \\ 0 & 0 & 0 & I \end{pmatrix} \begin{pmatrix} I & 0 & 0 & 0 \\ 0 & \mathcal{G} & 0 & 0 \\ 0 & 0 & I & 0 \\ 0 & 0 & 0 & I \end{pmatrix} = P_{\mathcal{G}}^{(1)} P_{\mathcal{G}}^{(2)}, \tag{19}$$

$$P_{\mathcal{F}} = \begin{pmatrix} I & 0 & 0 & 0 \\ 0 & I & 0 & 0 \\ 0 & \mathcal{D} & I & 0 \\ 0 & 0 & 0 & I \end{pmatrix} \begin{pmatrix} I & 0 & 0 & 0 \\ 0 & I & 0 & 0 \\ 0 & 0 & I & 0 \\ -\dfrac{\gamma}{\beta\Delta t} I_{\Gamma^s} & 0 & 0 & I \end{pmatrix} \begin{pmatrix} I & 0 & 0 & 0 \\ 0 & I & 0 & 0 \\ 0 & 0 & \mathcal{F} & I_{\Gamma^f}^T \\ 0 & 0 & I_{\Gamma^f} & 0 \end{pmatrix} = P_{\mathcal{F}}^{(1)} P_{\mathcal{F}}^{(2)} P_{\mathcal{F}}^{(3)}. \tag{20}$$

The factors $P_{\mathcal{G}}^{(1)}$, $P_{\mathcal{F}}^{(1)}$ and $P_{\mathcal{F}}^{(2)}$ can be inverted exactly (and cost-free). Since $\mathcal{S}$ and $\mathcal{G}$ appear (as diagonal blocks) in different factors, physics-specific ad-hoc preconditioners can be efficiently used to approximate their inverses. Unfortunately, this is only partially true for the fluid subproblem $\mathcal{F}$ whose saddle point structure features the additional presence of the two coupling blocks I_{Γ^f} and $I_{\Gamma^f}^T$.

We remark that factorization (18) has already been used in [14], where after factorization, the inverses of $P_{\mathcal{S}}$, $P_{\mathcal{G}}$ and $P_{\mathcal{F}}$ were approximated by the one level algebraic additive Schwarz method [53, 57].

The novelty of this paper with respect to [14] consists in operating a static condensation on the interface fluid variables, and in using SIMPLE [19, 48, 49, 21, 22, 51, 52] to precondition the resulting reduced fluid matrix. In fact, we notice that according to the (further) factorization (20) of $P_{\mathcal{F}}$, the critical term is $P_{\mathcal{F}}^{(3)}$ which corresponds to a linearized Navier-Stokes problem with additional constraints. Our goal is to replace

it, after static condensation of the interface variables, by a convenient approximation built on an efficient SIMPLE preconditioner.

We point out that our static condensation of the interface variables is operated at the level of the fluid preconditioner. A different approach, see e.g. [26, 44], consists in removing the interface variables directly from the set of unknowns of the FSI problem (14). In Section 4.2 we will show that the corresponding block preconditioner introduced in [26] differs from ours.

4.1. Static condensation and approximation of $P_{\mathcal{F}}^{(3)}$ based on SIMPLE preconditioner

By static condensation of the degrees of freedom related to the Lagrange multipliers $\boldsymbol{\lambda}$, we show that the application of $P_{\mathcal{F}}^{(3)}$ is equivalent to solving a linearized Navier-Stokes problem with Dirichlet boundary conditions at the fluid-structure interface. Let us extract from $P_{\mathcal{F}}^{(3)}$ the blocks associated to the fluid and the coupling parts, yielding the following saddle-point problem:

$$\begin{pmatrix} \begin{pmatrix} \mathcal{K} & \mathcal{B}^T \\ \mathcal{B} & 0 \end{pmatrix} & I_{\Gamma^f}^T \\ I_{\Gamma^f} & 0 \end{pmatrix} \begin{pmatrix} \delta\mathbf{u}_{f,k}^{n+1} \\ \delta p_{f,k}^{n+1} \\ \delta\boldsymbol{\lambda}_k^{n+1} \end{pmatrix} = \begin{pmatrix} \mathbf{r}_{\mathbf{u},k}^{n+1} \\ \mathbf{r}_{p,k}^{n+1} \\ \mathbf{r}_{\boldsymbol{\lambda},k}^{n+1} \end{pmatrix}, \tag{21}$$

where we highlighted the block structure of $\mathcal{F}$

$$\mathcal{F} = \begin{pmatrix} \mathcal{K} & \mathcal{B}^T \\ \mathcal{B} & 0 \end{pmatrix}, \tag{22}$$

being $\mathcal{K}$, $\mathcal{B}$, and $\mathcal{B}^T$ the block matrices of $\mathcal{F}$ representing the linearized advection-diffusion-reaction, the divergence, and the gradient operators, respectively. We notice that the coupling matrix I_{Γ^f} features the following structure:

$$I_{\Gamma^f} = (I_{\Gamma^{u_f}} \vdots 0),$$

where $I_{\Gamma^{u_f}}$ is the restriction of the fluid velocity to the interface Γ. The linear system (21) is equivalent to:

$$\begin{cases} \mathcal{K}\delta\mathbf{u}_{f,k}^{n+1} + \mathcal{B}^T\delta p_{f,k}^{n+1} + I_{\Gamma^{u_f}}^T\delta\boldsymbol{\lambda}_k^{n+1} = \mathbf{r}_{\mathbf{u},k}^{n+1}, & \text{(23a)} \\ \mathcal{B}\delta\mathbf{u}_{f,k}^{n+1} = \mathbf{r}_{p,k}^{n+1}, & \text{(23b)} \\ I_{\Gamma^{u_f}}\delta\mathbf{u}_{f,k}^{n+1} = \mathbf{r}_{\boldsymbol{\lambda},k}^{n+1}. & \text{(23c)} \end{cases}$$

By splitting $\delta\mathbf{u}_{f,k}^{n+1}$ into its internal component $\delta\mathbf{u}_{f,k,i}^{n+1}$ and its interface component $\delta\mathbf{u}_{f,k,\Gamma}^{n+1}$, the first step consists in eliminating the variables $\delta\mathbf{u}_{f,k,\Gamma}^{n+1}$ using Eq. (23c).

The second step proceeds by replacing the newly computed variables $\delta\mathbf{u}_{f,k,\Gamma}^{n+1}$ into (23a) and (23b). This leads to a new system from which the variable $\delta\boldsymbol{\lambda}_k^{n+1}$ can be formally eliminated, yielding:

$$\delta\boldsymbol{\lambda}_k^{n+1} = I_{\Gamma^{u_f}} I_{\Gamma^{u_f}}^T \delta\boldsymbol{\lambda}_k^{n+1} = I_{\Gamma^{u_f}}(\mathbf{r}_{\mathbf{u}_f,k}^{n+1} - \mathcal{K}\delta\mathbf{u}_{f,k}^{n+1} - \mathcal{B}^T\delta p_{f,k}^{n+1}). \tag{24}$$

The remaining equations consist then in the system

$$\begin{pmatrix} \mathcal{K}_{ii} & \mathcal{B}_i^T \\ \mathcal{B}_i & 0 \end{pmatrix} \begin{pmatrix} \delta\mathbf{u}_{f,k,i}^{n+1} \\ \delta p_{f,k}^{n+1} \end{pmatrix} = \begin{pmatrix} \mathbf{r}_{\mathbf{u},k,i}^{n+1} - \mathcal{K}_{i\Gamma}\delta\mathbf{u}_{f,k,\Gamma}^{n+1} \\ \mathbf{r}_{p,k}^{n+1} - \mathcal{B}_\Gamma\delta\mathbf{u}_{f,k,\Gamma}^{n+1} \end{pmatrix}, \tag{25}$$

where $\mathcal{K}_{ii}$ and $\mathcal{B}_i^T$ are the matrices representing the linearized advection-diffusion-reaction and gradient terms, respectively, restricted to the internal degrees of freedom $\delta\mathbf{u}_{f,k,i}^{n+1}$. Eq. (25) features the classical saddle-point form of a system associated to the linearized Navier-Stokes equations.

At this point we replace the matrix in (25) by its approximation based on SIMPLE preconditioner

$$\mathcal{F} \cong \widetilde{\mathcal{F}} = \begin{pmatrix} \mathcal{K}_{ii} & 0 \\ \mathcal{B}_i & -\widetilde{S} \end{pmatrix} \begin{pmatrix} I & D^{-1}\mathcal{B}_i^T \\ 0 & I \end{pmatrix}, \tag{26}$$

where D is the diagonal of $\mathcal{K}_{ii}$, and $\widetilde{S} = \mathcal{B}_i D^{-1} \mathcal{B}_i^T$ the approximated Shur complement of (25). In the application of FaCSI, the inverses of $\mathcal{S}$, $\mathcal{G}$, $\mathcal{K}_{ii}$ and $\widetilde{S}$ are approximated by associated efficient preconditioners denoted by $\mathcal{H}_{\mathcal{S}}$, $\mathcal{H}_{\mathcal{G}}$, $\mathcal{H}_{\mathcal{K}_{ii}}$ and $\mathcal{H}_{\widetilde{S}}$, respectively, based, e.g., on domain decomposition or the multigrid method. This concludes the construction of the preconditioner FaCSI for J_{FSI}, which takes the following final form:

$$P_{FaCSI} = P_{\mathcal{S}}^{ap} \cdot P_{\mathcal{G}}^{ap} \cdot P_{\mathcal{F}}^{ap}, \tag{27}$$

where:

$$P_{\mathcal{S}}^{ap} = \begin{pmatrix} \mathcal{H}_{\mathcal{S}} & 0 & 0 & 0 \\ 0 & I & 0 & 0 \\ 0 & 0 & I & 0 \\ 0 & 0 & 0 & I \end{pmatrix}, \quad P_{\mathcal{G}}^{ap} = \begin{pmatrix} I & 0 & 0 & 0 \\ -I_{\Gamma^s} & \mathcal{H}_{\mathcal{G}} & 0 & 0 \\ 0 & 0 & I & 0 \\ 0 & 0 & 0 & I \end{pmatrix} \tag{28}$$

and

$$P_{\mathcal{F}}^{ap} = \begin{pmatrix} I & 0 & 0 & 0 \\ 0 & I & 0 & 0 \\ 0 & \mathcal{D} & \begin{pmatrix} I & 0 & 0 \\ 0 & I_\Gamma & 0 \\ 0 & 0 & I \end{pmatrix} & \begin{pmatrix} 0 \\ 0 \\ 0 \end{pmatrix} \\ -\dfrac{\gamma}{\beta\Delta t} I_{\Gamma^s} & 0 & \begin{pmatrix} 0 & 0 & 0 \end{pmatrix} & I \end{pmatrix} \begin{pmatrix} I & 0 & 0 & 0 \\ 0 & I & 0 & 0 \\ 0 & 0 & \begin{pmatrix} I & 0 & 0 \\ 0 & 0 & 0 \\ 0 & 0 & I \end{pmatrix} & \begin{pmatrix} 0 \\ I_\Gamma \\ 0 \end{pmatrix} \\ 0 & 0 & \begin{pmatrix} 0 & I_\Gamma & 0 \end{pmatrix} & I \end{pmatrix} \begin{pmatrix} I & 0 & 0 & 0 \\ 0 & I & 0 & 0 \\ 0 & 0 & \begin{pmatrix} \mathcal{H}_{\mathcal{K}_{ii}} & \mathcal{K}_{i\Gamma} & 0 \\ 0 & I_\Gamma & 0 \\ \mathcal{B}_i & \mathcal{B}_\Gamma & -\mathcal{H}_{\widetilde{S}} \end{pmatrix} & \begin{pmatrix} 0 \\ I_\Gamma \\ 0 \end{pmatrix} \\ 0 & 0 & \begin{pmatrix} 0 & 0 & 0 \end{pmatrix} & I \end{pmatrix}$$

$$\begin{pmatrix} I & 0 & 0 & 0 \\ 0 & I & 0 & 0 \\ 0 & 0 & \begin{pmatrix} I & 0 & D^{-1}\mathcal{B}_i^T \\ 0 & I_\Gamma & 0 \\ 0 & 0 & I \end{pmatrix} & \begin{pmatrix} 0 \\ I_\Gamma \\ 0 \end{pmatrix} \\ 0 & 0 & \begin{pmatrix} 0 & 0 & 0 \end{pmatrix} & I \end{pmatrix} \begin{pmatrix} I & 0 & 0 & 0 \\ 0 & I & 0 & 0 \\ 0 & 0 & \begin{pmatrix} I & 0 & 0 \\ 0 & I_\Gamma & 0 \\ 0 & 0 & I \end{pmatrix} & \begin{pmatrix} 0 \\ 0 \\ 0 \end{pmatrix} \\ 0 & 0 & \begin{pmatrix} \mathcal{K}_{\Gamma i} & \mathcal{K}_{\Gamma\Gamma} & \mathcal{B}_\Gamma^T \end{pmatrix} & I \end{pmatrix}. \tag{29}$$

For the sake of clarity, we point out that, for a given residual $\mathbf{r} = (\mathbf{r}_{\mathbf{d}_s}, \mathbf{r}_{\mathbf{d}_f}, \mathbf{r}_{\mathbf{u}_f}, \mathbf{r}_{p_f}, \mathbf{r}_{\boldsymbol{\lambda}})^T$, the application of our preconditioner amounts to solve $P_{FaCSI}\mathbf{w} = \mathbf{r}$, therefore involving the following steps:

1. Application of $(P_{\mathcal{S}}^{ap})^{-1}$: $\mathbf{w}_{\mathbf{d}_s} = \mathcal{H}_{\mathcal{S}}^{-1}\mathbf{r}_{\mathbf{d}_s}$.
2. Application of $(P_{\mathcal{G}}^{ap})^{-1}$: $\mathbf{w}_{\mathbf{d}_f} = \mathcal{H}_{\mathcal{G}}^{-1}(\mathbf{r}_{\mathbf{d}_f} + I_{\Gamma^s}\mathbf{w}_{\mathbf{d}_s})$.
3. Application of $(P_{\mathcal{F}}^{ap})^{-1}$: compute $\mathbf{z}_F = \mathbf{r}_F - \mathcal{D}\mathbf{w}_{\mathbf{d}_f}$ and $\mathbf{z}_{\boldsymbol{\lambda}} = \mathbf{r}_\lambda + \dfrac{\gamma}{\beta\Delta t} I_{\Gamma^s}\mathbf{w}_{\mathbf{d}_s}$. Then, after denoting by $\mathbf{w}_{\mathbf{u}}$ and $\mathbf{w}_p$, $\mathbf{z}_{\mathbf{u}}$ and $\mathbf{z}_p$ the velocity and pressure components of $\mathbf{w}_F$ and $\mathbf{z}_F$, respectively, thanks to (23c) we set $\mathbf{z}_{\mathbf{u},\Gamma} = \mathbf{z}_{\boldsymbol{\lambda}}$. The application of the SIMPLE preconditioner involves:
   a) $\mathbf{y}_{\mathbf{u},i} = \mathcal{H}_{\mathcal{K}_{ii}}^{-1}(\mathbf{z}_{\mathbf{u},i} - \mathcal{K}_{i\Gamma}\mathbf{z}_{\mathbf{u},\Gamma})$,
   b) $\mathbf{w}_p = \mathcal{H}_{\widetilde{S}}^{-1}(\mathcal{B}_i\mathbf{y}_{\mathbf{u},i} - \mathbf{z}_p + \mathcal{B}_\Gamma\mathbf{z}_{\mathbf{u},\Gamma})$,

c) $\mathbf{w}_{\mathbf{u}} = (\mathbf{w}_{\mathbf{u},i}, \mathbf{w}_{\mathbf{u},\Gamma})^T = (\mathbf{y}_{\mathbf{u},i} - D^{-1}\mathcal{B}_i^T \mathbf{w}_p, \mathbf{z}_{\mathbf{u},\Gamma})^T$.

Finally, we compute $\mathbf{w}_{\boldsymbol{\lambda}} = I_{\Gamma^{u_f}}(\mathbf{z}_{\mathbf{u}} - \mathcal{K}\mathbf{w}_{\mathbf{u}} - \mathcal{B}^T \mathbf{w}_p)$.

Remark 2. In [30] a similar factorization as in Eq. (18) was used, and a SIMPLE preconditioner was exploited to directly approximate the factor $P_{\mathcal{F}}^{(3)}$. However, no static condensation was used to eliminate the interface fluid variables, yielding therefore to a different preconditioner. In Section 5.2 we show that static condensation substancially increases the performance with respect to the version proposed in [30].

4.2. Comparison with other condensed formulations

In [26] the authors consider a condensed formulation of the coupled FSI problem for which the unknowns are $\hat{\mathbf{d}}_{s,i}$, $\hat{\mathbf{d}}_{f,i}$, $\mathbf{u}_f$ and p_f, being $\hat{\mathbf{d}}_{s,i}$ and $\hat{\mathbf{d}}_{f,i}$ the structure and fluid mesh displacement associated to the internal degrees of freedom, respectively. In particular, the vector of Lagrange multipliers is condensed into the structural displacement unknowns at the interface. In our case $\boldsymbol{\lambda}$ is condensed into the fluid velocity.

The block Gauss-Seidel preconditioner proposed in [26] (see Eq. (43) in [26]) reads:

$$M = \begin{pmatrix} \mathcal{S}_{ii} & 0 & \begin{pmatrix} 0 & 0 \end{pmatrix} \\ 0 & \mathcal{G}_{ii} & \begin{pmatrix} 0 & 0 \end{pmatrix} \\ \begin{pmatrix} \mathcal{S}_{\Gamma i} \\ 0 \end{pmatrix} & \begin{pmatrix} \mathcal{D}_{\Gamma i} \\ \mathcal{D}_{ii} \end{pmatrix} & \begin{pmatrix} \delta\mathcal{S}_{\Gamma\Gamma} + \mathcal{F}_{\Gamma\Gamma} + \delta\mathcal{D}_{\Gamma\Gamma} & \mathcal{F}_{\Gamma i} \\ \mathcal{F}_{i\Gamma} + \delta\mathcal{D}_{i\Gamma} & \mathcal{F}_{ii} \end{pmatrix} \end{pmatrix} \tag{30}$$

In (30) each block matrix (i.e. $\mathcal{S}$, $\mathcal{G}$, $\mathcal{F}$ and $\mathcal{D}$) is split into its internal (index i) and interface (index Γ) components; δ is a factor which converts displacement into velocity.

By comparing (17) with (30) we observe that the two block preconditioners are different. More specifically, the nature of the subproblems change: in (30) the structure bears a Dirichlet problem, the ALE is still of Dirichlet type and decoupled from the structure, while the fluid is a Neumann problem. In FaCSI, the structure bears a Neumann problem, the ALE is of Dirichlet type and it is coupled with the structure while the fluid is of Dirichlet type. Furthermore, we notice that due to the condensed formulation adopted in [26], we observe that the fluid block in (30) slightly differs from ours at the interface.

The aforemetioned differences may be summarized by stating that the block Gauss-Seidel preconditioner devised in [26] is of Neumann-Dirichlet type while FaCSI is of Dirichlet-Neumann type. In [18] a comparison of the performance of Dirichlet-Neumann, Neumann-Dirichlet and Neumann-Neumann preconditioners for the Steklov-Poincaré formulation of the FSI problem was carried out. There, it was shown that the Dirichlet-Neumann preconditioner was the most efficient in terms of requested both CPU time and linear solver iterations.

5. Numerical results

We test our FSI preconditioner on two different test cases: the first is an FSI example in which we study the fluid flow in a straight flexible tube, the second consists in the simulation of the hemodynamics in a femoropopliteal bypass. We measure the weak and strong scalability of the proposed preconditioner, namely the wall time and iterations count.

The FSI problem is discretized by a Fully Implicit (FI) second order scheme in time and space. The resulting nonlinear system is solved by the exact Newton method using tolerance $\epsilon = 10^{-6}$ in (16). We solve the linearized problem at each Newton iteration by the right preconditioned GMRES method [54] which is never restarted. Since in our case the matrices associated to the harmonic extension and the structure

are constant throughout the simulation, their preconditioners $\mathcal{H}_{\mathcal{S}}$ and $\mathcal{H}_{\mathcal{G}}$ are computed once and stored. Conversely, we recompute the preconditioner associated to the fluid problem, namely $\mathcal{H}_{\mathcal{K}_{ii}}$ and $\mathcal{H}_{\widetilde{S}}$, at each Newton iteration. The initial guess for Newton is set to zero to guarantee a comparable iterations count from one timestep to another. In practice, better choices can be made, e.g., by taking as initial guess an extrapolation of the solutions at the previous time steps.

We have implemented our parallel algorithm in LifeV [1], an open-source C++ finite element library which makes intensive use of Trilinos [34]. Our linear iterative solver (GMRES) is based on the Belos package [9]. In this work we consider preconditioners $\mathcal{H}_{\mathcal{S}}$, $\mathcal{H}_{\mathcal{G}}$, $\mathcal{H}_{\mathcal{K}_{ii}}$ and $\mathcal{H}_{\widetilde{S}}$ based on either the one level Algebraic Additive Schwarz (AAS) method implemented in Ifpack [55] or on Algebraic Multigrid (AMG) via ML [27]. Whenever mesh coarsening is required, aggregates are computed using METIS/ParMETIS [37, 38]. All the computations reported in this work have been made on Piz Dora at CSCS, a Cray XC40 machine whose main technical specifications are reported in Table 1.

Number of compute nodes	1'256
Number of compute cores	30'144, 24 per compute node
Processor type	Dual-socket Intel Xeon E5-2690 v3, 2.5 GHz
Processors shared memory per node	64 GB
Network	Dragonfly interconnect

Table 1: Piz Dora (Cray XC40) technical data.

5.1. FSI in a straight flexible tube

Our first numerical example is a benchmark problem proposed in [46] and numerically solved, e.g., in [14, 17, 26, 59]. The geometry of the fluid consists in a straight cylinder of length $L = 5$ cm and radius $R = 0.5$ cm, surrounded by a structure with uniform thickness $t = 0.1$ cm. A constant normal stress $\boldsymbol{\sigma} \cdot \mathbf{n} = 1.33 \times 10^4$ dyne/cm^2 is applied at the fluid inflow for $t \leq 0.003$ s, while a homogeneous Neumann boundary condition is used at the fluid outflow. The structure is clamped at both the ends. The fluid is characterized by a density $\rho_f = 1.0$ g/cm^3 and a dynamic viscosity $\mu_f = 0.03$ g/(cm s) while the structure by a density $\rho_s = 1.2$ g/cm^3, Poisson's ratio $\nu_s = 0.3$ and Young's modulus $E_s = 3 \times 10^6$ dyne/cm^2.

We are interested in studying the weak and strong scalability performance of FaCSI when different choices for $\mathcal{H}_{\mathcal{S}}$, $\mathcal{H}_{\mathcal{G}}$, $\mathcal{H}_{\mathcal{K}_{ii}}$ and $\mathcal{H}_{\widetilde{S}}$ are considered. In Table 2 we report the different configurations adopted to customize FaCSI for the analysis. As reported in Table 2, three different configurations are studied: in the first (set A) we consider the one level AAS preconditioner with an algebraic overlap $\delta = 2$ (i.e., roughly two times the mesh size h) for $\mathcal{H}_{\mathcal{S}}$, $\mathcal{H}_{\mathcal{G}}$, $\mathcal{H}_{\mathcal{K}_{ii}}$ and $\mathcal{H}_{\widetilde{S}}$. In set B, the 3 level AMG method is used: we consider a symmetric Gauss-Seidel smoother (ω is the damping parameter) for levels 1 and 2 while at the coarsest level, i.e. level 3, the problem is solved exactly. Set C is a combination of set A and set B: we make use of the AAS method for $\mathcal{H}_{\mathcal{S}}$, $\mathcal{H}_{\mathcal{G}}$, while the 3 level AMG method is used for $\mathcal{H}_{\mathcal{K}_{ii}}$ and $\mathcal{H}_{\widetilde{S}}$. We remark that the exact local subdomain solves for AAS as well as the exact coarse solve of the AMG preconditioner are carried out by LU factorization using the library MUMPS [2, 3].

To validate the solver implemented, in Figure 2 we show a post-processing of the numerical solution obtained by simulating 100 time steps: the results reported well compare with those in [17, 23, 26, 59].

Configuration	Preconditioner	Approximation
set A	$\mathcal{H}_{\mathcal{S}}$	1 level AAS
	$\mathcal{H}_{\mathcal{G}}$	1 level AAS
	$\mathcal{H}_{\mathcal{K}_{ii}}$	1 level AAS
	$\mathcal{H}_{\widetilde{\mathcal{S}}}$	1 level AAS
set B	$\mathcal{H}_{\mathcal{S}}$	3 level AMG, ω=0.79
	$\mathcal{H}_{\mathcal{G}}$	3 level AMG, ω=1.0
	$\mathcal{H}_{\mathcal{K}_{ii}}$	3 level AMG, ω=0.69
	$\mathcal{H}_{\widetilde{\mathcal{S}}}$	3 level AMG, ω=1.0
set C	$\mathcal{H}_{\mathcal{S}}$	1 level AAS
	$\mathcal{H}_{\mathcal{G}}$	1 level AAS
	$\mathcal{H}_{\mathcal{K}_{ii}}$	3 level AMG, ω=0.69
	$\mathcal{H}_{\widetilde{\mathcal{S}}}$	3 level AMG, ω=1.0

Table 2: Different configurations of FaCSI considered for this analysis.

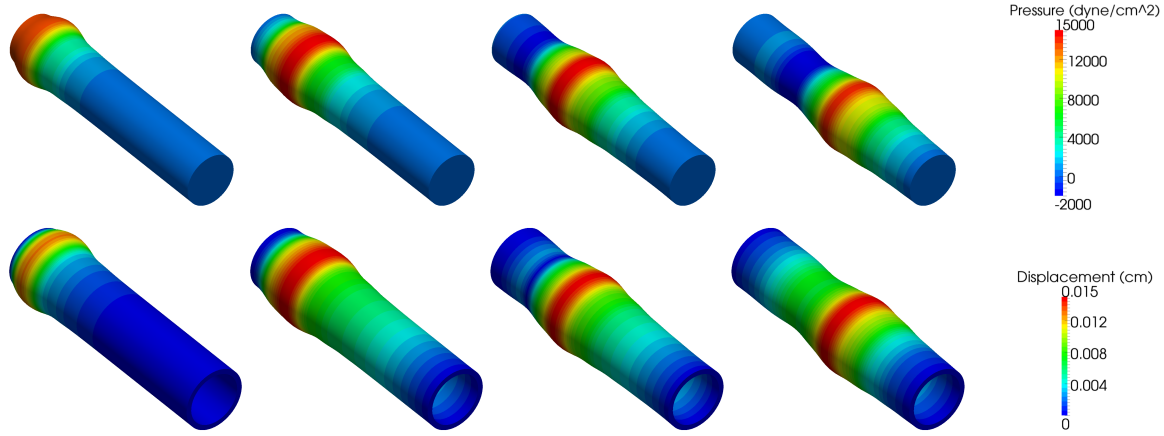

(a) t = 2 ms. (b) t = 4 ms. (c) t = 6 ms. (d) t = 8 ms.

Figure 2: On the top row we show the pressure wave propagation throughout the deformed fluid domain while on the bottom one we report the structural displacement at different time instants. The deformation is magnified by a factor 10 for visualization purpose only.

In Table 3 and 4 we report the information concerning the meshes used in our simulations and the correponding number of degrees of freedom.

5.1.1. Weak and strong scalability of FaCSI

The strong and weak scalability performance of FaCSI are tested by solving the straight flexible tube example using three sets of fluid-structure meshes (that are conforming at the interface) of increasing refinement and three different configurations of FaCSI. In Figure 3 and 4 we report the weak and strong scalability results, respectively (consisting in average values over the first 10 time steps simulated).

	Fluid		Structure	
	# Vertices	# Tetrahedra	# Vertices	# Tetrahedra
Mesh # 1	210'090	1'202'040	65'424	292'320
Mesh # 2	559'471	3'228'960	191'080	913'920
Mesh # 3	841'341	4'880'640	300'456	1'497'600

Table 3: Details of the meshes used for the straight cylinder example.

	Fluid DoF	Structure DoF	Coupling DoF	Geometry DoF	Total
Mesh # 1	5'134'050	1'369'030	195'576	4'923'960	11'622'616
Mesh # 2	13'728'971	4'119'980	456'114	13'169'500	31'474'595
Mesh # 3	20'696'341	6'599'740	598'104	19'855'000	47'749'185

Table 4: Straight flexible tube test case: number of Degrees of Freedom (DoF).

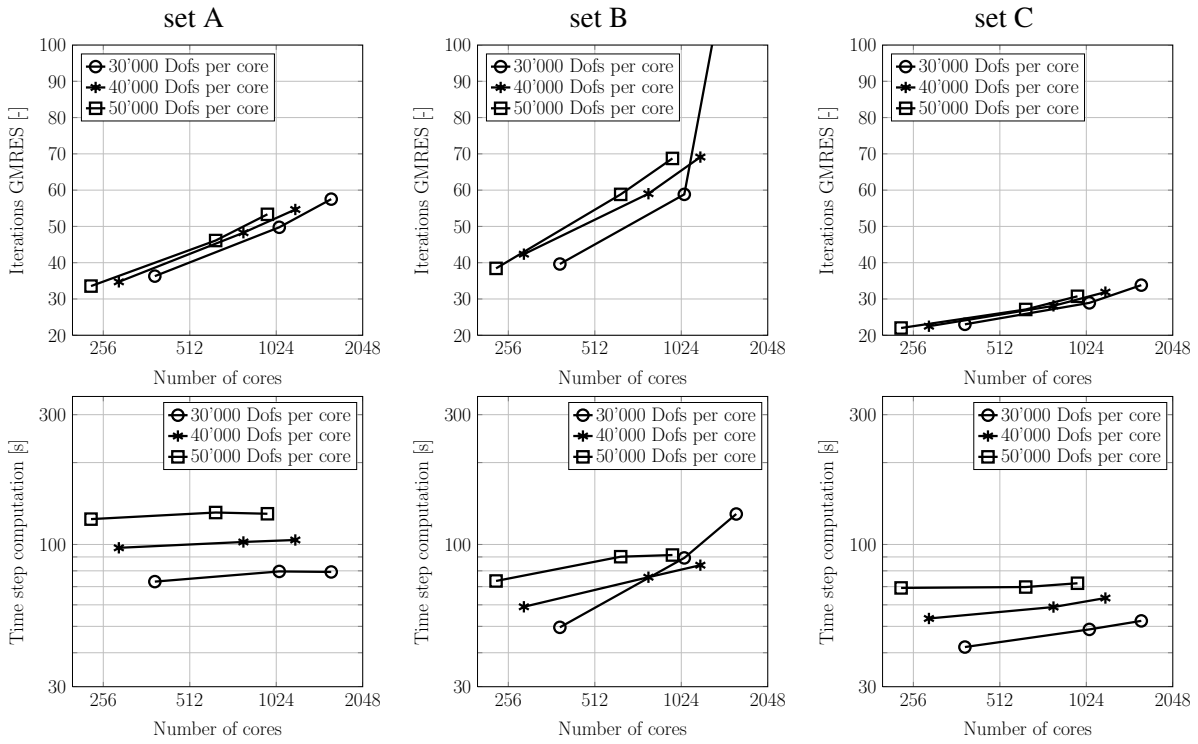

Figure 3: Weak scalability results obtained using three different configurations of FaCSI (see Table 2).

In the weak scalability study, the problem size (workload) assigned to each core is kept constant. In our investigation we address the cases of 30'000, 40'000 and 50'000 degrees of freedom per core. In terms of GMRES iterations (first row of Figure 3), we notice that FaCSI configured with set C performs better with respect to configurations of set A and set B. In fact, set C yields an iteration count which mildly depends on both the mesh size (along each curve the number of iterations vary from roughly 22 to 34 iterations) and the

number of degrees of freedom per core since the three curves almost overlap. Configuration of set A leads to a number of linear iterations which on the one hand mildly depends on the core workload but on the other is rather sensitive to the mesh size (along each curve the iterations vary from roughly 30 to 60 iterations). We observe that FaCSI configured with set B yields iteration counts that are affected by both the mesh size and the number of degrees of freedom per core. We focus now on the weak scalability of the time to compute a single time step (second row of Figure 3). FaCSI configured with set A leads to computational times that are weakly scalable for all the core workloads taken into account. Nevertheless, comparing the results obtained by set A with those generated with set B and C, we notice that set A is the most computational expensive. In particular, we highlight that the time to compute a time step using set C with 50'000 Dofs per core (which is roughly 70 s) is smaller than the one with workload 30'000 Dofs per core using set A (that is roughly 80 s). FaCSI configured with set B is not weakly scalable as the timings obtained vary significantly (in particular when 30'000 Dofs per core are used). Using set C, we notice that the time to compute a single time step is weakly scalable for a core workload of 50'000 Dofs while for 30'000 and 40'000 it increases with the cores count as the time spent by communication is larger than the actual one associated to the relatively small amount of computational work required on each individual core.

In Figure 4 we show the strong scalability results obtained. In the first row of Figure 4 we report the number of GMRES iterations, in the second row the time to build the preconditoner of the fluid problem, in the third row the time to solve the linear system while in the fourth row the time to compute a single time step. We remark that in the second row of Figure 4 we report the time to build only the preconditioner for the fluid problem: in fact, since the harmonic extension and the structure matrices are constant throughout the simulation, their preconditioners are built only once and stored at the beginning.

In terms of linear solver iterations we notice that FaCSI configured with set C performs better than both set A and set B (in line with what we observed in the study of the weak scalability). Indeed, for all the 3 meshes considered, we notice that the use of set C leads to a number of linear solver iterations that is the lowest and which is less affected by the number of cores utilized.

Regarding the time to build the fluid preconditioner, although set A leads to strongly scalable results (the red curve behaves almost as the black one of the ideal scaling), we notice that up to 2'048 cores set B and set C allows for a remarkably faster computation w.r.t. set A. For instance, when a small number of cores is used, the construction of the fluid preconditioner by the algebraic multigrid method (set B and set C) is roughly ten times lower then the one of the overlapping algebraic additive Schwarz (set A). Nevertheless, although AMG leads to a very fast construction of the preconditioner, we notice that in our numerical experiments its construction scales up to 512 cores (on Mesh # 3). We remark that the curves in the second row of Figure 4 associated to set B and set C are overlapping since their settings for the fluid problem are the same (see Table 2). In terms of time to solve the linear system, we notice that with the configurations of set A FaCSI scales up to 2'048 cores, with set B until 512 cores whereas using set C linear scaling is obtained up to 1'024 cores. It is noteworthy that until 1'024 cores the solution of the linear system carried out by FaCSI customized by set C is the fastest (in particular almost two times faster than set A). The last row of Figure 4 shows the strong scalability of the time to compute a single time step. Strong scalability of FaCSI customized with set A, set B and set C is observed up to 4'096, 1'024 and 2'048 cores, respectively. Also in this case we notice that until FaCSI configured with set C scales linearly, it is the fastest. For instance, until 2'048 cores on Mesh # 3, we remark that the computational times associated to set A are roughly the same of those obtained by set C using, for the latter, half of the cores.

Based on the analysis presented so far we conclude that FaCSI customized with set C (i.e. using the one level AAS method for both $\mathcal{H}_{\mathcal{S}}$ and $\mathcal{H}_{\mathcal{G}}$, and the 3 level AMG method for $\mathcal{H}_{\mathcal{K}_{ii}}$ and $\mathcal{H}_{\widetilde{\mathcal{S}}}$) is the most computationally efficient and robust with respect to the mesh size among all the configurations taken into

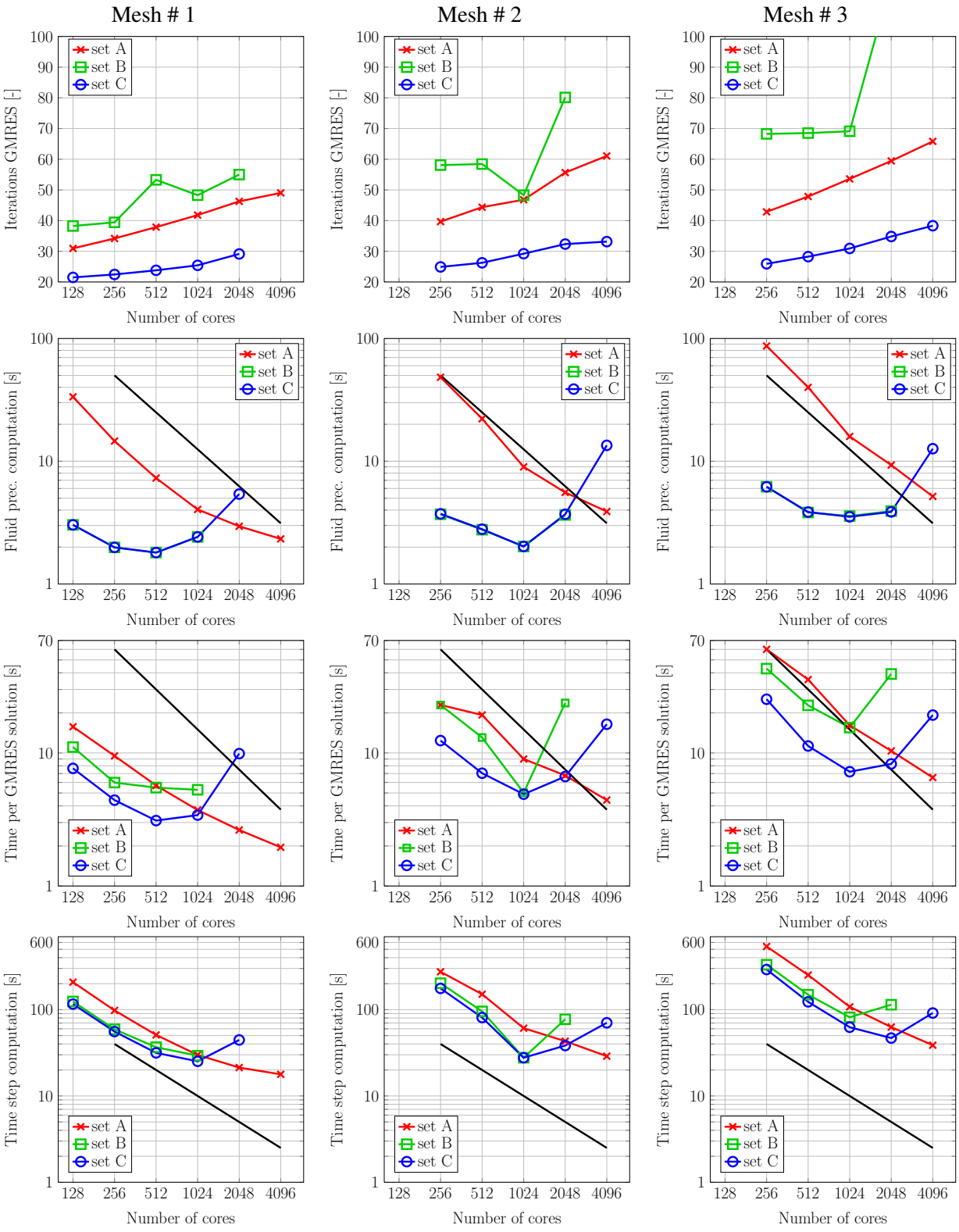

Figure 4: Strong scalability results obtained on meshes of increasing refinement (see Table 3). Black lines denote ideal scaling.

account in our analysis.

5.1.2. Comparison of FaCSI with other preconditioners

We compare the performance of FaCSI (hereafter configured using set C) with some state of the art preconditioners for FSI. In particular, we compare with the two preconditioners based on algebraic multigrid techniques proposed in [26] and the one level overlapping additive Schwarz preconditioner proposed in [59]. In both [59, 26] the numerical example of the pressure wave propagation throughout a flexible tube is addressed. To carry out the comparison with [26] (in which hexahedral elements were used, whereas we use tetrahedra) we solve the FSI problem using both first order and second order space discretizations (denoted as "P1" and "P2" in Table 5). The comparison with [59] is carried out using the "P1" discretization (same settings of [59]). We remark that in the "P1" case, the fluid problem is stabilized using the same stabilization of [59].

For both the "P1" and "P2" discretizations the fluid-structure meshes have been generated such that the numbers of degrees of freedom of the fluid, structure and geometry fields are similar to those reported in [26] (see Table III discretization *pw3*). Discretization "P1" in Table 5 has almost the same number of degrees of freedom of the finer one used in [59] (that is 3.08×10^6). The comparisons of the results obtained by FaCSI with those reported in [26] and [59] are shown in Table 6 and in Figure 5, respectively: we notice that FaCSI well compare with both the preconditioners taken into account for the analysis.

Discretization	Fluid DoF	Structure DoF	Coupling DoF	Geometry DoF	Total
"P1"	1'539'226	456'120	75'180	1'154'420	3'224'946
"P2"	1'568'223	458'280	90'744	1'503'280	3'620'527

Table 5: Degrees of freedom of the discretized FSI problem for the comparisons with [26, 59].

	# unknowns	CPUs	# GMRES
BGS(AMG), *pw3*	3'063'312	16	41.77
AMG(BGS), *pw3*	3'063'312	16	30.29
FaCSI, "P1"	3'224'946	16	23.24
FaCSI, "P2"	3'620'527	16	17.09

Table 6: Comparison of FaCSI with the preconditioners proposed in [26]. Note that # GMRES is the average number of GMRES iterations per Newton step (that is 3 both for us and [26]).

5.2. Femoropopliteal bypass

We consider a hemodynamic simulation in a femoropopliteal bypass. This problem has already been investigated in [42]. The geometric model of the femoropopliteal bypass was obtained through a 3T MRI scanner while the computational unstructured meshes used in our simulations were generated using VMTK and Gmsh [29]. We consider the blood characterized by a density $\rho_f = 1$ g/cm^3 and by a dynamic viscosity $\mu_f = 0.035$ g/(cm s). The physical parameters of the vessel wall are set as follows: the Young's modulus is $E_s = 4 \times 10^6$ dyne/cm^2, the Poisson's ratio is $\nu_s = 0.45$, and the density is $\rho_s = 1.2$ g/cm^3. The boundaries of the computational domain are labeled as illustrated in Figure 7. We impose patient-specific measured flow rates on Γ^f_{in} and Γ^f_{out} while homogeneous Dirichlet conditions are applied at the occluded branch Γ^f_{occl}. The structure is clamped at the inlets and the outlet rings Γ^s_{in}, Γ^s_{occl} and Γ^s_{out} where we impose $\hat{\mathbf{d}}_s = 0$.

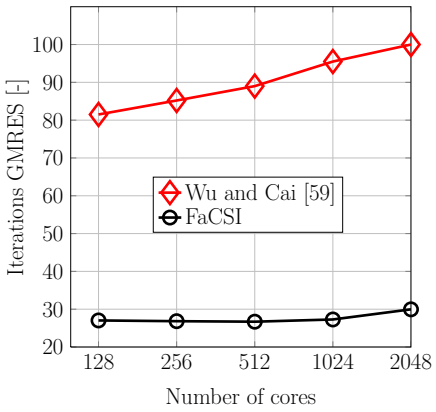

Figure 5: Comparison of FaCSI (using the "P1" discretization, see Table 5) with the overlapping additive Schwarz preconditioner proposed in [59] (red curve taken from right-most plot in Figure 4 of [59]).

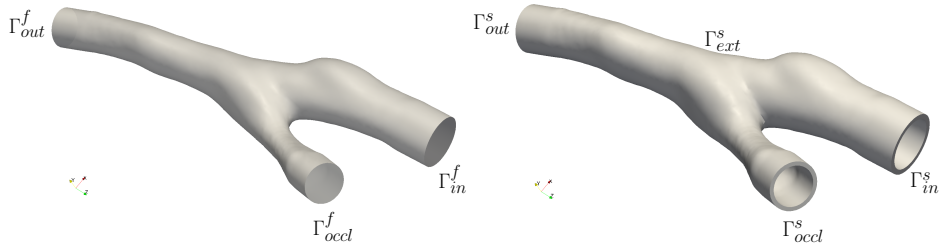

(a) Fluid domain. (b) Structure domain.

Figure 6: Femoropopliteal bypass test case: labels of the boundaries.

Homogenous Neumann boundary conditions are imposed at the outer surface of the vessel Γ^s_{ext} The time step used is $\Delta t = 0.001$ s.

In our numerical simulations, we study the robustness of the proposed preconditioner with respect to the mesh size for a varying number of cores utilized. To analyze the robustness of the preconditioner proposed with respect to the mesh size, we consider two set of fluid-structure meshes that are conforming at the interface, whose number of vertices and elements are summarized in Table 7. Figure 7 shows the computational meshes generated for the femoropopliteal bypass. In Table 8 we report the information concerning the number of degrees of freedom associated to the meshes used.

	Fluid		Structure	
	# Vertices	# Tetrahedra	# Vertices	# Tetrahedra
Mesh # 1	354'178	2'153'476	113'380	508'374
Mesh # 2	2'768'791	17'247'246	451'900	2'029'878

Table 7: Details of the coarse and fine meshes used for the femoropopliteal bypass example.

The strong scalability results of FaCSI (configured with set C of Table 2) are reported in Figure 8. In Figure 10 we show a post-processing of the numerical solution computed using Mesh # 2 at three time instances during the third heart beat simulated.

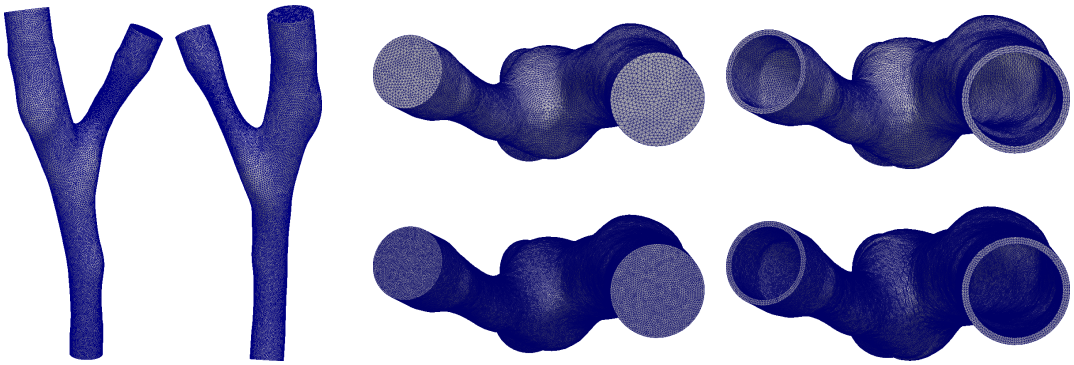

(a) Front and back view, Mesh #1.

(b) Top view: Mesh # 1 (first row) and Mesh # 2 (second row).

Figure 7: Meshes generated for the femoropopliteal bypass test case.

	Fluid DoF	Structure DoF	Coupling DoF	Geometry DoF	Total
Mesh # 1	9'029'128	2'376'720	338'295	8'674'950	20'419'093
Mesh # 2	71'480'725	9'481'350	1'352'020	68'711'934	151'026'029

Table 8: Femoropopliteal bypass test case: number of degrees of freedom.

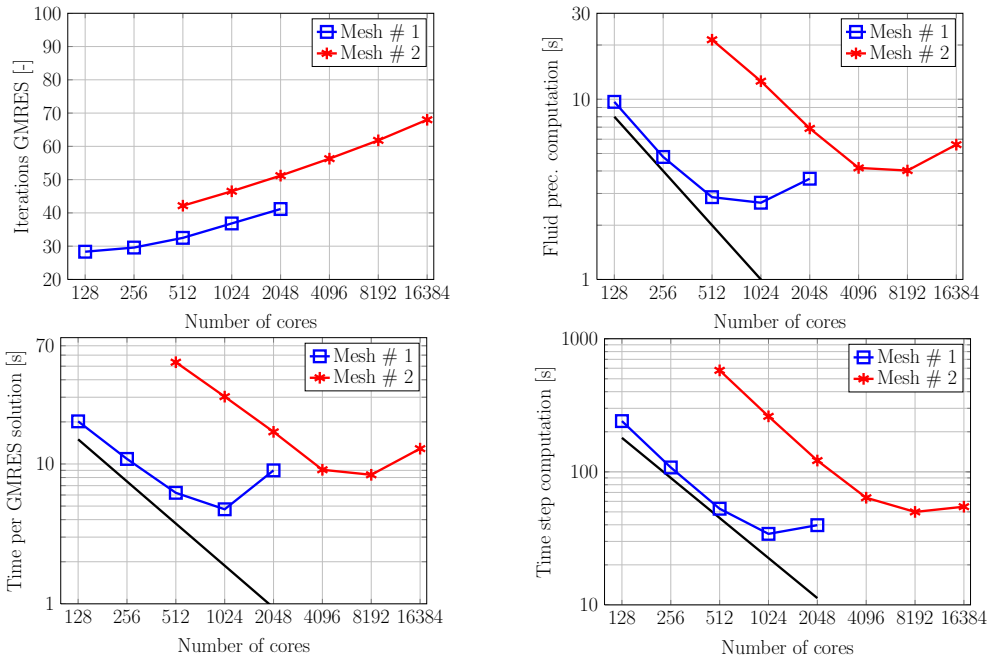

Figure 8: Strong scalability results for the femoropopliteal bypass example.

As shown in Figure 8, we observe the robustness of FaCSI with respect to both the mesh size and the number of cores utilized. Indeed, on the smaller mesh (Mesh # 1) the number of linear solver iterations ranges from roughly 30 (with 128 cores) to 40 iterations (with 2'048 cores). On the larger mesh (Mesh #

2) the GMRES iterations increase from roughly 40 (using 512 cores) to 70 (with 16'384 cores). On the smaller mesh the strong scalability of the time to compute a single time step is close to the ideal scaling up to 512 cores while on the larger mesh is close to the be linear until 4'096 cores. We observe that on both Mesh # 1 and Mesh # 2, FaCSI scales almost linearly until the local number of degrees of freedom per core is roughly 40'000. For instance, on Mesh # 1 using 512 cores and on Mesh # 2 using 4'096 cores the single core workload is approximately 40'000. When the number of degrees of freedom per core is lower than 40'000 the communication occurring for the construction of the preconditioner and the solution of the linear system (as shown in Figure 8) dominates the relatively small amount of computational work performed by each single core. This behavior is in line with the weak scalability results obtained in Section 5.1.1 (see Figure 3), where we observed that FaCSI (configured by set C) was weakly scalable up to 40'000 degrees of freedom per core.

We recall that in [30] a similar factorization as in Eq. (18) was used, and a SIMPLE preconditioner was exploited to directly approximate the factor $P_{\mathcal{F}}^{(3)}$. However, no static condensation was used to eliminate the interface fluid variables, yielding therefore to a different preconditioner (that in [30] is called FSI-SIMPLE).

For the sake of illustration, in Figure 9 we show the number of linear solver iterations reported in [30] to solve the femoropopliteal bypass example, with the same fluid and solid geometries and the same boundary conditions adopted here. The results of Figure 9 refer to a discretization of the FSI problem of 8'142'612 degrees of freedom, hence coarser than Mesh # 1 used in our Table 8. Moreover, we notice that the results of Figure 9 were obtained using subiterations for the application of the preconditioner FSI-SIMPLE. Subiterations allow to impose more accurately the preconditioner and in general ensure that the number of iterations remains almost constant as the number of cores utilized increases. We remark that the FaCSI preconditioner does not require subiterations.

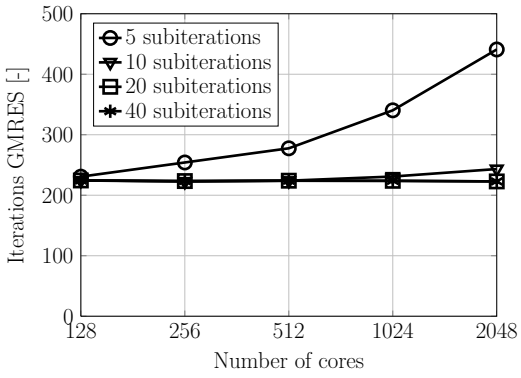

Figure 9: Femoropopliteal bypass example: number of linear solver iterations reported in [30], Figure 5.18(c). The FSI problem is discretized using 8'142'612 degrees of freedom.

By comparing the results of Figure 9 with the number of linear solver iterations associated to Mesh # 1 reported in Figure 8, we notice that the performance of FaCSI are much better than those of FSI-SIMPLE [30] (without static condensation). In particular, it is noteworthy that the number of linear solver iterations of FaCSI (which ranges from roughly 30 to 40 on Mesh # 1) is remarkably smaller that those of FSI-SIMPLE (roughly 220) when 20 or 40 subiterations are used for the latter.

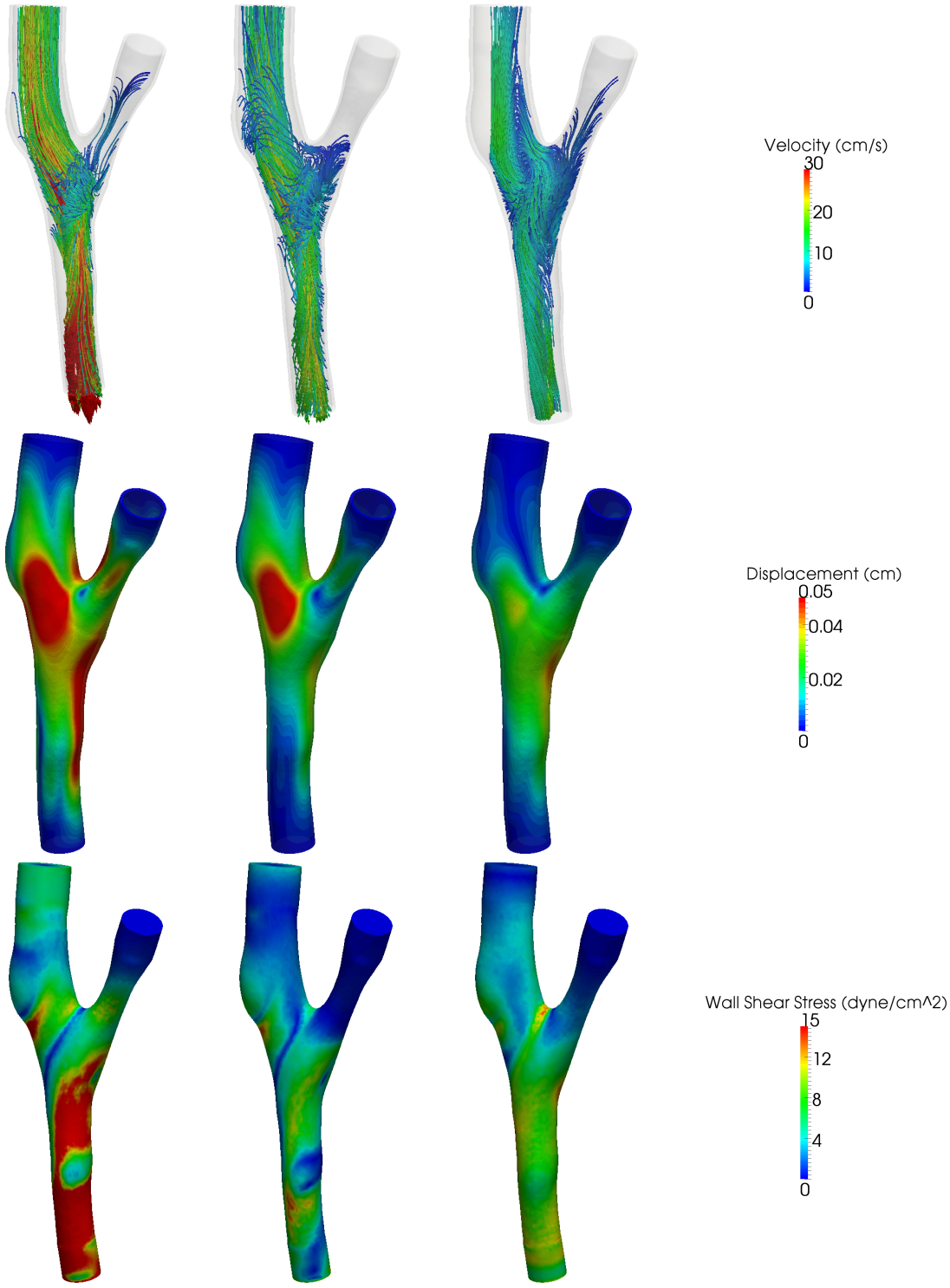

Figure 10: Post-processing of the results at time t = 1.8 s (left), 1.9 s (middle) and 2.0 s (right). Time t = 1.8 s coincides with the systolic peak of the third heart beat simulated. In the top row we show the streamlines of the fluid flow, in the middle row the magnitude of the structural displacement while in the bottom row the Wall Shear Stress.

6. Conclusion

We proposed a block preconditioner for FSI simulations that takes advantage of physics-specific ad-hoc preconditioners available for each subproblem (structure, geometry and fluid). We considered a second order discretization scheme in space and time and we solved the FSI problem using a monolithic coupling scheme wherein the nonlinearities are treated fully-implicitly. An analysis of the strong and weak scalability properties of FaCSI was carried out by using different preconditioners (additive Schwarz and multigrid) for the structure, geometry and fluid problems. Our analysis shows that the the most efficient choice consists in using the 1 level algebraic additive Schwarz preconditioners for the structure and geometry problems, together with the 3 level algebraic multigrid method for the fluid. We tested the efficiency of the proposed block preconditioner on a benchmark cylindrical configuration and on a realistic geometry of hemodynamics. We showed that FaCSI compares succesfully with state of the art preconditioners for FSI. Our parallel algorithm showed scalability up to thousands of cores utilized on realistic problems where about 150 millions of degrees of freedom were used, featuring also robustness with respect to mesh size.

Acknowledgements

We acknowledge the Swiss Platform for High-Performance and High-Productivity Computing (HP2C). The research of D. Forti was supported by the Swiss National Foundation (SNF), project no. 140184. We gratefully acknowledge the CSCS for providing us the CPU resources under project ID s635. We acknowlegde the Center for Advanced Modelling Science (CADMOS) for the use of the Lemanicus Blue Gene/Q supercomputer. We also thank the LifeV community.

References

[1] LifeV user manual. http://www.lifev.org, 2010.

[2] P. R. Amestoy, I. S. Duff, J. Koster, J. Y. L'Excellent. A fully asynchronous multifrontal solver using distributed dynamic scheduling. *SIAM J. Matrix Anal. Appl.*, 23(1):15–41, 2001.

[3] P. R. Amestoy, A. Guermouche, J. Y. L'Excellent, S. Pralet. Hybrid scheduling for the parallel solution of linear systems. *Parallel Comput.*, 32(2), 136–156, 2006.

[4] S. Badia, F. Nobile, and C. Vergara. Fluid-structure partitioned procedures based on Robin transmission conditions. *J. Comput. Phys.*, 227(14):7027–7051, 2008.

[5] S. Badia, F. Nobile, and C. Vergara. Robin-Robin preconditioned Krylov methods for fluid-structure interaction problems. *Comput. Methods Appl. Mech. Engrg.*, 198(33-36):2768–2784, 2009.

[6] S. Badia, A. Quaini, and A. Quarteroni. Modular vs. non-modular preconditioners for fluid-structure systems with large added-mass effect. *Comput. Methods Appl. Mech. Engrg.*, 197(49-50):4216–4232, 2008.

[7] S. Badia, A. Quaini, and A. Quarteroni. Splitting methods based on algebraic factorization for fluid-structure interaction. *SIAM J. Sci. Comput.*, 30(4):1778–1805, 2008.

[8] A. T. Barker and X.-C. Cai. Scalable parallel methods for monolithic coupling in fluid-structure interaction with application to blood flow modeling. *J. Comput. Phys.*, 229(3):642–659, 2010.

[9] E. Bavier, M. Hoemmen, S. Rajamanickam, and H. Thornquist. Amesos2 and Belos: Direct and iterative solvers for large sparse linear systems. *Scientific Programming*, 20(3):241–255, 2012.

[10] Y. Bazilevs, V. M. Calo, T. J. R. Hughes, and Y. Zhang. Isogeometric fluid-structure interaction: theory, algorithms, and computations. *Comput. Mech.*, 43(1):3–37, 2008.

[11] Y. Bazilevs, K. Takizawa, and T.E. Tezduyar. *Computational Fluid–Structure Interaction. Methods and Applications*. Wiley Series in Computational Mechanics. Wiley, 2013.

[12] P. Causin, J. F. Gerbeau, and F. Nobile. Added-mass effect in the design of partitioned algorithms for fluid-structure problems. *Comput. Methods Appl. Mech. Engrg.*, 194(42-44):4506–4527, 2005.

[13] G. H. Cottet, E. Maitre, and T. Milcent. Eulerian formulation and level set models for incompressible fluid-structure interaction. *M2AN Math. Model. Numer. Anal.*, 42(3):471–492, 2008.

[14] P. Crosetto, S. Deparis, G. Fourestey, and A. Quarteroni. Parallel algorithms for fluid-structure interaction problems in haemodynamics. *SIAM J. Sci. Comput.*, 33(4):1598–1622, 2011.
[15] P. Crosetto, P. Reymond, S. Deparis, D. Kontaxakis, N. Stergiopulos, and A. Quarteroni. Fluid-structure interaction simulation of aortic blood flow. *Comput. Fluids*, 43:46–57, 2011.
[16] J. Degroote, K.-J. Bathe, and J. Vierendeels. Performance of a new partitioned procedure versus a monolithic procedure in fluidstructure interaction. *Comput. Struct.*, 87:793–801, 2009.
[17] S. Deparis, M. Discacciati, G. Fourestey, and A. Quarteroni. Fluid-structure algorithms based on Steklov-Poincaré operators. *Comput. Methods Appl. Mech. Engrg.*, 195(41-43):5797–5812, 2006.
[18] S. Deparis, D. Forti, A. Heinlein, A. Klawonn, A. Quarteroni, and O. Rheinbach. A Comparison of Preconditioners for the Steklov-Poincaré Formulation of the Fluid-Structure Coupling in Hemodynamics. *PAMM*, 15(1):93–94, 2015.
[19] S. Deparis, G. Grandperrin, and A. Quarteroni. Parallel preconditioners for the unsteady Navier–Stokes equations and applications to hemodynamics simulations. *Comput. Fluids*, 92:253–273, 2013.
[20] W. G. Dettmer and D. Perić. A fully implicit computational strategy for strongly coupled fluidsolid interaction. *Arch. Comput. Methods Engrg.*, 14(3):205–247, 2007.
[21] H. Elman, V. E. Howle, J. Shadid, R. Shuttleworth, and R. Tuminaro. Block preconditioners based on approximate commutators. *SIAM J. Sci. Comput.*, 27(5):1651–1668, 2006.
[22] H. Elman, V. E. Howle, J. Shadid, R. Shuttleworth, and R. Tuminaro. A taxonomy and comparison of parallel block multilevel preconditioners for the incompressible Navier-Stokes equations. *J. Comput. Phys.*, 227(3):1790–1808, 2008.
[23] M. A. Fernández and M. Moubachir. A Newton method using exact jacobians for solving fluidstructure coupling. *Comput. Struct.*, 83:127–142, 2005.
[24] L. Formaggia, A. Quarteroni, and A. Veneziani, editors. *Cardiovascular mathematics*, volume 1 of *MS&A. Modeling, Simulation and Applications*. Springer-Verlag Italia, Milan, 2009. Modeling and simulation of the circulatory system.
[25] D. Forti and L. Dedè. Semi–implicit BDF time discretization of the Navier–Stokes equations with VMS–LES modeling in High Performance Computing framework. *Comput. Fluids*, 117:168–182, 2015.
[26] M. W. Gee, U. Küttler and W. A. Wall. Truly monolithic algebraic multigrid for fluid-structure interaction. *Int. J. Numer. Engng*, 85:987–1016, 2011.
[27] M. W. Gee, C. M. Siefer, J. J. Hu, R. S. Tuminaro, and M. G. Sala. *ML* 5.0 Smoothed Aggregation User's Guide, Sandia National Laboratories, 2006.
[28] J. F. Gerbeau and M. Vidrascu. A quasi-Newton algorithm based on a reduced model for fluid-structure interaction problems in blood flows. *M2AN Math. Model. Numer. Anal.*, 37(4):631–647, 2003.
[29] C. Geuzaine and J. F. Remacle. Gmsh reference manual. Technical report, University of Liège, 2010. http://geuz.org/gmsh/doc/texinfo/gmsh.pdf.
[30] G. Grandperrin. *Parallel Preconditioners for Navier-Stokes Equations and Fluid-Structure Interaction Problems: Application to Hemodynamics*. PhD thesis, EPFL, 2013.
[31] M. Heil. An efficient solver for the fully coupled solution of large-displacement fluid–structure interaction problems. *Comput. Methods Appl. Mech. Engrg.*, 193(1-2):1–23, 2004.
[32] M. Heil, A. L. Hazel, and J. Boyle. Solvers for large–displacement fluid–structure interaction problems: segregated versus monolithic approaches. *Comput. Mech.*, 43(1):91–101, 2008.
[33] T. J. R. Hughes. The finite element method: linear static and dynamic finite element analysis. *Courier Corporation*, 2012.
[34] M. A. Heroux, R. A. Bartlett, V. E. Howle, R. J. Hoekstra, J. J. Hu, T. G. Kolda, R. B. Lehoucq, K. R. Long, R. P. Pawlowski, E. T. Phipps, A. G. Salinger, H. K. Thornquist, R. S. Tuminaro, J. M. Willenbring, A. Williams, and K. S. Stanley. An overview of the trilinos project. *ACM Trans. Math. Softw.*, 31(3):397–423, 2005.
[35] R. A. Horn and C. R. Johnson. *Matrix Analysis*. Cambridge University Press, 1990.
[36] R. A. Horn and C. R. Johnson. *Topics in matrix analysis*. Cambridge University Press, Cambridge, 1991.
[37] G. Karypis, K. Schloegel, and V. Kumar. METIS: A Software Package for Partitioning Unstructured Graphs, Partitioning Meshes, and Computing Fill-Reducing Orderings of Sparse Matrices. Technical report, Univ MN., 1998.
[38] G. Karypis, K. Schloegel, and V. Kumar. ParMETIS: Parallel Graph Partitioning and Sparse Matrix Ordering library. Technical report, Univ MN., 2003.
[39] U. Küttler, M. W. Gee, C. Förster, A. Comerford, and W. A. Wall. Coupling strategies for biomedical fluid-structure interaction problems. *Int. J. Numer. Methods Biomed. Eng.*, 26(3-4):305–321, 2010.
[40] U. Küttler and W. A. Wall. Fixed-point fluid–structure interaction solvers with dynamic relaxation. *Comput. Mech.*, 43(1):61–72, 2008.
[41] P. Le Tallec and J. Mouro. Fluid structure interaction with large structural displacements. *Comput. Methods Appl. Mech. Engrg.*, 190:3039–3067, 2001.
[42] E. Marchandise, P. Crosetto, C. Geuzaine, J. F. Remacle, and E. Sauvage. Quality open source mesh generation for cardiovascular flow simulations. In D. Ambrosi, A. Quarteroni, and G. Rozza, editors, *Modeling of Physiological Flows*, volume 5

of *MS&A Modeling, Simulation and Applications*, pages 395–414. Springer Milan, 2012.
[43] H. G. Matthies, R. Niekamp, and J. Steindorf. Algorithms for strong coupling procedures. *Comput. Methods Appl. Mech. Engrg.*, 195(17-18):2028–2049, 2006.
[44] M. Mayr, T. Klöppel, W. A. Wall, and M. W. Gee. A temporal consistent monolithic approach to fluid-structure interaction enabling single field predictors. 2015. *SIAM J. Sci. Comput.*, 37(1):B30–B59, 2015.
[45] R. Mittal and G. Iaccarino. Immersed boundary methods. In *Annual review of fluid mechanics. Vol. 37*, volume 37 of *Annu. Rev. Fluid Mech.*, pages 239–261. Annual Reviews, Palo Alto, CA, 2005.
[46] F. Nobile. *Numerical approximation of fluid-structure interaction problems with application to haemodynamics*. PhD thesis, SB, Lausanne, 2001.
[47] F. Nobile, M. Pozzoli, and C. Vergara. Inexact accurate partitioned algorithms for fluidstructure interaction problems with finite elasticity in haemodynamics. *J. Comput. Phys.*, 273(0):598 – 617, 2014.
[48] S. V. Patankar and D. B. Spalding. A calculation procedure for heat, mass and momentum transfer in three dimensional parabolic flows. *Int. J. Heat Mass Transfer*, 15:1787–1806, 1972.
[49] M. Pernice and M. D. Tocci. A multigrid-preconditioned Newton-Krylov method for the incompressible Navier-Stokes equations. *SIAM J. Sci. Comput.*, 23(2):398–418 (electronic), 2001. Copper Mountain Conference (2000).
[50] C. S. Peskin. The immersed boundary method. *Acta Numer.*, 11:479–517, 2002.
[51] M. Rehman, C. Vuik and G. Segal. SIMPLE-type preconditioners for the Oseen problem. *Int. J. Num. Meth. in Fluids*, 61:432–452, 2009.
[52] M. Rehman, C. Vuik and G. Segal. Preconditioners for the steady incompressible Navier-Stokes problem. *International Journal of Applied Mathematics*, 38:223–232, 2008.
[53] A. Quarteroni and A. Valli. *Domain decomposition methods for partial differential equations*. Numerical Mathematics and Scientific Computation. The Clarendon Press - Oxford University Press, New York, 1999. Oxford Science Publications.
[54] Y. Saad and M. H. Schultz. GMRES: a generalized minimal residual algorithm for solving nonsymmetric linear systems. *SIAM J. Sci. Statist. Comput.*, 7(3):856–869, 1986.
[55] M. Sala and M. Heroux. Robust Algebraic Preconditioners with IFPACK 3.0, Sandia National Laboratories, 2005.
[56] T. E. Tezduyar, S. Sathe, and K. Stein. Solution techniques for the fully discretized equations in computation of fluid-structure interactions with the space-time formulations. *Comput. Methods Appl. Mech. Engrg.*, 195(41-43):5743–5753, 2006.
[57] A. Toselli and O. Widlund. *Domain decomposition methods—algorithms and theory*, volume 34 of *Springer Series in Computational Mathematics*. Springer-Verlag, Berlin, 2005.
[58] H. Wang, J. Chessa, W. K. Liu, and T. Belytschko. The immersed/fictitious element method for fluid-structure interaction: volumetric consistency, compressibility and thin members. *Int. J. Numer. Meth. Eng.*, 74(1):32–55, 2008.
[59] Y. Wu and X. C. Cai. A fully implicit domain decomposition based ALE framework for three-dimensional fluid-structure interaction with application in blood flow computation. *J. Comput. Phys.*, 258:524–537, 2014.

Recent publications:

MATHEMATICS INSTITUTE OF COMPUTATIONAL SCIENCE AND ENGINEERING
Section of Mathematics
Ecole Polytechnique Fédérale
CH-1015 Lausanne

01.2015 PENG CHEN, ALFIO QUARTERONI, GIANLUIGI ROZZA:
Reduced order methods for uncertainty quantification problems

02.2015 FEDERICO NEGRI, ANDREA MANZONI, DAVID AMSALLEM:
Efficient model reduction of parametrized systems by matrix discrete empirical interpolation

03.2015 GIOVANNI MIGLIORATI, FABIO NOBILE, RAÚL TEMPONE:
Convergence estimate in probability and in expectation for discrete least squares with noisy evaluations at random points

04.2015 FABIO NOBILE, LORENZO TAMELLINI, FRANCESCO TESEI, RAÚL TEMPONE:
An adaptive sparse grid alorithm for elliptic PDEs with lognormal diffusion coefficent

05.2015 MICHAEL STEINLECHNER:
Riemannian optimization for high-dimensional tensor completion

06.2015 V. R. KOSTIĆ, A. MIEDLAR, LJ. CVETKOVIĆ:
An algorithm for computing minimal Geršgorin sets

07.2015 ANDREA BARTEZZAGHI, LUCA DEDÈ, ALFIO QUARTERONI:
Isogeometric analysis of high order partial differential equations on surfaces

08.2015 IVAN FUMAGALLI, ANDREA MANZONI, NICOLA PAROLINI, MARCO VERANI:
Reduced basis approximation and a posteriori error estimates for parametrized elliptic eigenvalue problems

09.2015 DAVIDE FORTI, LUCA DEDÈ:
Semi-implicit BDF time discretization of the Navier-Stokes equations with VMS-LES modeling in a High Performance Computing framework

10.2015 PETAR SIRKOVIĆ, DANIEL KRESSNER:
Subspace acceleration for large-scale parameter-dependent Hermitian eigenproblems

11.2015 FEDERICO NEGRI:
A model order reduction framework for parametrized nonlinear PDE-constrained optimization

12.2015 ANNA TAGLIABUE, LUCA DEDÈ. ALFIO QUARTERONI:
Nitsche's method for parabolic partial differential equations with mixed time varying boundary conditions

13.2015 NEW SIMONE DEPARIS, DAVIDE FORTI, GWENOL GRANDPERRIN, ALFIO QUARTERONI:
FaCSI: A block parallel preconditioner for fluid-structure interaction in hemodynamics